Interferometric Encoders for Linear Displacement Metrology

Von der Fakultät für Maschinenbau
der Technischen Universität Carolo-Wilhelmina zu Braunschweig
zur Erlangung der Würde
eines Doktor-Ingenieurs (Dr.-Ing.)
genehmigte Dissertation

von: Jun Guan
aus (Geburtsort): Henan, V.R.China

eingereicht am: 30.05.2013
mündliche Prüfung am: 05.09.2013

Gutachter:
Prof. Dr.-Ing. Rainer Tutsch, Institut für Produktionsmesstechnik
Prof. Dr. rer. nat Andreas Hangleiter, Institut für Angewandte Physik
Dr. Jens Flügge, Physikalisch-Technische Bundesanstalt, Fachbereich 5.2

2013

Zusammenfassung

Eine der anspruchsvollsten Anforderungen der linearen Verschiebungsmessungen liegt derzeit in der Positionierung von Wafertischen für Lithografiemaschinen, die Messbereiche von mehreren hundert Millimetern und Messunsicherheiten im Bereich von einigen Nanometern bis hin zu Sub-Nanometern erfordern. Momentan können nur Interferometer und interferometrische Encoder diese Anforderungen erfüllen. Im Vergleich zu Encodern benötigen Interferometer jedoch sehr genau definierte Umgebungsbedingungen, um diese Anforderungen zu erfüllen. Deswegen werden interferometrische Encoder immer populärer.

In dieser Arbeit wurde ein dreikanaliger homodyner (3KH) Encoder, ein zweidimensionaler homodyner (2DH) Encoder sowie ein differentieller heterodyner (DH) Encoder entwickelt.

Der 3KH Encoder hatte drei Kanäle, die verschiedene Beugungsordnungen verwenden, wobei die gleiche Position auf einem Gittermaßstab gemessen wurde. Das Design des 3KH Encoder war dahingehend konzipiert wurden, um mögliche unterschiedliche Messunsicherheiten, hervorgerufen durch die Korrelationen zwischen Unvollkommenheiten des Maßstabs und der verschiedenen Beugungsordnungen, zu untersuchen. Wenn zur Signalauswertung ein HEIDENHAIN EIB741 verwendet wurde, hatte der 3KH Encoder periodische Nichtlinearitäten (PN) von ±50 pm im Kanal 1, ±150 pm im Kanal 2 und ±70 pm im Kanal 3. Desweiteren wurde eine selbstentwickelte Auswerteelektronik und eine

Heydemannkorrektur genutzt, wodurch ein PN von ±10 pm erzielt wurde.

Der 2DH Encoder wurde prinzipiell ausgelegt, um Verschiebungen sowohl entlang des eindimensionalen Gittermaßstabes als auch der orthogonalen Richtung zu bestimmen. Das Prinzip wurde durch Experiment nachgewiesen.

Der DH Encoder basierte auf einem differenziellen Messprinzip und war gezielt zur Vermeidung von Polarisationsmischung entwickelt worden. Es konnte ohne Korrektur ein PN von ±30 pm bestimmt werden. Zudem wurden eine Stabilität von 38 pm (σ) über 30 Sekunden und 100 pm (σ) über eine Stunde gemessen.

Abstract

Currently one of the most challenging demands on linear displacement metrology comes from positioning of the wafer stages of the lithography machine tools, which requires measurement ranges of hundreds of millimeters and measurement uncertainties of several nanometers and even below. At present, only displacement interferometers and interferometric encoders can be managed to meet these requirements; but to do so, interferometers need very strict environmental controlling if not vacuum. Therefore more and more attentions are paid to interferometric encoders due to their lower sensitivities to the refraction-index fluctuations of ambient air and the wavelength deviations.

In this work, a three-channel homodyne interferometric (TCHOI) encoder, a two-dimensional homodyne interferometric (2DHI) encoder and a differential heterodyne interferometric (DIHEI) encoder were developed:

The TCHOI encoder had three channels which used different diffraction orders but measured the same position on the scale grating. The design of this TCHOI encoder provided an opportunity to study the suspected different measurement uncertainties caused by the correlations between the imperfections of the grating scale and different diffraction orders. The periodic nonlinearities of the TCHOI encoder were ± 50 pm in channel1, ± 150 pm in channel2 and ± 70 pm in channel3, when HEIDENHAIN EIB741 was employed. As a home-developed phase meter and off-line correction were used, its channel1 had a periodic nonlinearity of ± 10 pm.

The 2DHI encoder was designed to measure the displacements in X- and Z- directions with one dimensional grating scale. Its principle was proven by the proof-of-principle experiment.

The DIHEI encoder was based on differential measurement principle and a polarization-mixing-avoiding strategy. It had a periodic nonlinearity of less than ± 30 pm (without correction) and system stabilities of 38 pm (σ) and 100 pm (σ) over 30 seconds and one hour respectively.

Table of Contents

1. Introduction

1.1. Background

In mechanics, displacement is a measure of both the distance and direction that an object travels. Every displacement of a rigid body can be represented by a composition of linear displacement (translation) and angular displacement (rotation). Linear displacement is defined as the vector distance from the initial point to the final point along a line. Angular displacement is defined as the angle through which a rigid body has been rotated in a specified sense about a specified axis. In this thesis work only the metrology of linear displacement is focused on.

Automatic positioning is fundamental to industrial production. As one of the enabling technologies for automatic positioning, linear displacement metrology is always an important research field. At present, there are different types of displacement measurement sensors/instruments which can be used for automatic positioning.

According to the physical quantities those sensors are based on, basically linear displacement sensors can be divided into four categories: mechanical sensors, sonic/ultrasonic sensors, electrical/magnetic sensors and optical sensors, as shown in Table 1-1 in which only part of the commercially available linear displacement sensors are included.

Table 1-1. Part of the commercially available linear displacement sensors.

Type	Sensor	Principle	Characteristics
Mechanical sensor	Nozzle flappers	Convert displacements into pressure change of working fluid. Pressure change is measured.	Typical measurement range: ± 0.05 mm; Typical resolution: ± 0.01μm [1.1].
Sonic/ Ultrasonic sensor	Sonic and Ultrasonic sensors	The displacement of the measurand is converted into the flying-time change from the sonic/ultrasonic source to the receiver. Change of flying-time is measured.	Measurement range: up to dozens of meters; Typical linearity: ±1% FS (Full Scale) [1.2].
Electrical/ magnetic sensor	Capacitive sensors	The capacitance of a parallel capacitor C can be expressed as: $C = \varepsilon * A/d$. where ε is the dielectric constant of the medium between the plates, d is the separation between the plates and A is the cross-sectional area of the plates. Each of the three quantities can be varied to form a displacement transducer.	Typical measurement range: as small as 10^{-11} m up to as large as 1m [1.1]; Resolution: can be sub-nanometer [1.3, 1.4].
	Linear Variable Differential Transformer (LVDT)	It is essentially a three-coil variable reluctance transducer. When the core is located equidistantly with respect to its two secondary coils, the voltage output of this device will be zero. Otherwise output	Measurement range: up to hundreds of millimeters [1.5]; Typical linearity: up to ±0.1% FS [1.6].

		voltage will be proportional to the displacement of the core from the zero-voltage position.	
	Eddy current displacement sensors	An alternating current is generated in the sensing coil of the probe. This creates an alternating magnetic field which induces small currents (eddy currents) in the target material. The eddy currents create an opposing magnetic field which resists the field being generated by the probe coil. The interaction of the magnetic fields depends on the distance between the probe and the target. As the distance changes, the electronics sense the change in the field interaction.	Typical measurement range: up to dozens of millimeters; Typical linearity: ±0.2% FS; Tolerance of dirty environments. [1.7, 1.8]
	Linear Hall sensors	Linear Hall sensors utilize the Hall effect to sense the displacement. A simplest linear Hall sensor is composed of a Hall sensing element and a movable magnet, with an output proportional to the distance between those two.	Limited linear range, typically less than 25 mm [1.9]; Need to be calibrated by other displacement sensor or an artifact.
	Linear magnetic encoders	A linear magnetic encoder consists of a read head and a magnetic scale. As the read head passes over the encoded magnetic scale, it picks up the magnetic variations. Thus the relevant position between these two parts can be decided.	Measurement range: depends on the length of the scale; Typical resolution: more than 0.2 μm. [1.10, 1.11].
Optical sensor	Optical confocal sensors	A white light is focused onto the target surface by a multilens optical system. These lenses disperse the light into monochromatic stages (colors) along the measurement axis. The wavelength which is exactly focused on the target is used for	Measurement range: up to dozens of millimeters; Resolution: up to several nanometers. [1.12]

		the measurement. This light reflected from the target surface is transmitted from the probe, through a confocal aperture and onto a spectrometer. The spectral changes are processed and the displacement of the target can be calculated correspondingly.	
	Laser displacement sensors (triangulation sensors)	Laser diode projects a light beam onto the surface of the measurand. The back scattered light reflected from the measurand is projected onto the detector (a position sensitive device). The movement of the measurand will cause the light spot move on the detector, therefore the movement of the measurand can be detected.	Linearity and repeatability depends on the measurement range. Typically for 100mm measurement range, the related typical linearity is not less than ±0.03% FS [1.13].
	Displacement laser interferometers	The simplest form: A laser beam is split into two parts, one part strikes on the reference mirror which is fixed; another part is directed to the measurement mirror which is attached on the measurand. After these two parts being reflected back from reference and measurement mirrors, they are overlapped and interfere. The phase change of the interference signal theoretically results from the displacement of the measurand. After the phase change is measured, the relevant displacement is determined.	Measurement range: theoretically only limited by the laser coherence length; Measurement uncertainty: more sensitive to the fluctuation of the refractive index of ambient air and the frequency stabilization, compared to encoders [1.14-1.18]. Have the direct traceability to the SI definition of the meter [1.19]
	Linear optical encoders	A linear optical encoder has two basic parts: a grating scale and an	Measurement range:

		encoder head. When there is relative displacement between these two parts, detectable information will be generated correspondingly. There are basically three techniques to generate such detectable information: geometric masking, Moire effects and laser interference. Normally, linear optical encoders based on laser inference (known as Interferometric encoder) have the best performance.	depends on the length of the scale gratings; Measurement uncertainty: less sensitive to the fluctuations of ambient environment [1.14-1.18] compared to displacement interferometers, but with the influence of the imperfection of the grating scales.

Different application fields have different requirements on the performances of the linear displacement measurement systems/sensors: for the displacement sensors of elevators, millimeters of measurement uncertainties and resolutions are sufficient; but for displacement measurement sensors of diamond turning machines, normally the required resolutions are at sub-nanometer level. Currently one of the most challenging demands comes from the semiconductor manufacturing industry especially the displacement measurement systems of the wafer stages of the lithography machine tools, which require the measurement ranges of hundreds of millimeters and the measurement uncertainties of even several nanometers. At this moment only displacement interferometers and interferemetric encoders can meet these requirements. But along with the Critical Dimension (CD) shrinking and wafer size increasing [1.20], the requirements on the measurement uncertainties, repeatabilities and the measurement ranges of the displacement measurement systems are getting more

and more challenging. Due to the ever-stronger influence of the air turbulences caused by the ever-growing scanning velocities and dynamics of wafer stages and limitation of environment control, displacement interferometers are facing mounting difficulties to meet the requirements on measurement uncertainties, if they are not put into vacuum. But putting displacement interferometers into vacuum means drastic increasing of the total cost of ownership of the whole lithography machine tools. Therefore more and more attentions are paid to the interferometric encoders due to their lower sensitivities to the fluctuations of refraction index of ambient air and the wavelength variations of their light sources, compared to displacement interferometers [1.14-1.18].

There are already a number of commercial interferometric encoder products: encoder lineup of HEIDENHAIN [1.21, 1.22], MicroE Systems' Encoder family [1.23], NanoScale Linear Encoder and NanoGrid Planar Encoder from OPTRA [1.24], RENISHAW's encoder series [1.25] and so on. And also quite lots of experimental interferometric encoders from research works have been reported [1.26-1.37]. As for the principles and performances of those interferometric encoders in details, they will be described in the section 3.6. Up to now there is no reported interferometric encoder with sub-nanometer of measurement uncertainty which is demanded by the lithography machines in the near future. To this end, aiming at the interferometeric encoder with sub-nanometer measurement uncertainty and repeatability, in this work, a three-channel homodyne interferometric encoder and a differential heterodyne interferometric encoder were developed. After the major aspects of their performances were investigated, they were believed to have the

potentials to meet the requirements of sub-nanometer measurement uncertainty and sub-nanometer repeatability in the industrial applications.

Moreover, for some applications like high precision linear motors, which require out-of-plane measurements to compensate the related motion error [1.36], two-dimensional (one is in-plane another one is out-of-plane) measurements are demanded. Therefore, in this work, a two-dimensional (in-plane and out-of-plane) homodyne encoder was also devised and proven by the preliminary proof-of-principle experiment.

1.2. Motivation of this thesis work

Up to now there is no reported interferometric encoder with sub-nanometer of measurement uncertainty and repeatability (please refer to the section 3.6 for the proof.) which is demanded by the lithography machines in the near future. To this end, aiming at the interferometric encoder with sub-nanometer measurement uncertainty and repeatability, in this work, a three-channel homodyne interferometric encoder and a differential heterodyne interferometric encoder were developed. After the major aspects of their performances were investigated, they were believed to have the potentials to meet the requirements of sub-nanometer measurement uncertainty and sub-nanometer repeatability in the industrial applications.

A two-dimensional (one is in-plane another one is out-of-plane) homodyne encoder was also demonstrated aiming to meet the demand of some applications like the precision linear motor which

also need a out-of-plane displacement measurement to compensate the linear motion error[1.36].

1.3. Structure of this thesis

First of all, the background of this thesis work is given, followed by the introduction of the displacement interferometers. Then the background knowledge which relates to the interferometric encoder as well as the history and recent development will be talked about. Then my own works will be presented:

- A three-channel homodyne interferometric encoder;
- A two-dimensional homodyne interferometric encoder;
- A differential heterodyne interferometric encoder.

Finally, a conclusion will be drawn and some aspects which need to be done or considered next also will be briefly discussed.

References

[1.1]. Alan S Morris. Measurement and Instrumentation Principles (Third edition). Butterworth-Heinemann, ISBN 0 7506 5081 8

[1.2]. E4PA-N Ultrasonic Displacement Sensor. OMRON E4PA-N Catalog (web Edition), 2012.10

[1.3]. Capacitive Sensor Product Selector. LION PRECISION, http://www.lionprecision.com/capacitive-sensors/cap-products.html

[1.4]. Capacitive Position Sensors-Nanometrology Solutions-2007. PI (Physik Instrumente)

[1.5]. Sensotec Sensors. Pressure. Load. Force. Torque. Displacement. Vibration. Instrumentation. Full Line Catalog 27th Edition. Honeywell, 2006, LV-7

[1.6]. http://www.transtekinc.com/products/lvdt.html. April 2013

[1.7]. EDDY- CURRENT SENSORS Catalog. LION PRECISION, 04/2012

[1.8]. EDDY CURRENT PROBES. Waycon Positionsmesstechnik, 11/01/13

[1.9]. DAVID S. NYCE. LINEAR POSITION SENSORS Theory and Application. WILEY-INTERSCIENCE, ISBN 0-471-23326-9

[1.10]. MagLine | Magnetic Length and Angle Measurement Systems. SIKO GmbH, 01/2011

[1.11]. Flyer: Rotary, linear and ring magnetic encoders. RLS merilna tehnika d.o.o. A RENISHAW associate company

[1.12]. confocal DT Confocal chromatic measurement system. Micro-Epsilon, Y9761149-J031033SGO

[1.13]. Laser Triangulation Displacement Sensors. Micro-Epsilon, Y9766188-O051102GKE

[1.14]. Fred de Jong, Bert van der Pasch, Tom Castenmiller, Bert Vleeming, Richard Droste, Frank van de Mast. Enabling the

lithography roadmap: an immersion tool based on a Novel Stage Positioning System Proc. Of SPIE. 2009, 7274 (72741S): 1-10

[1.15]. Yuichi Shibazaki, Hirotaka Kohno, Masato Hamatani. An innovative platform for high-throughput high-accuracy lithography using a single wafer stage Proc. Of SPIE. 2009, 7274 (72741I): 1-12

[1.16]. Engelbertus Antonius Fransiscus VAN DER PASCH, Oirschot (NL); Emiel Jozef Melanie Eussen, Eindhoven (NL); Erik Roelof Loopstra, Eindhoven (NL) LITHOGRAPHIC APPARATUS AND DEVICE MANUFACTURING METHOD. United States Patent. 2011, Pub. No.: US 2011/0116066 A1

[1.17]. Leslie L. Deck, Middletown, CT (US); Peter J.De Groot, Middletown, CT (US); Michael Schroeder, East Hampton, CT (US). INTERFEROMETRIC ENCODER SYSTEMS United States Patent. 2012, Pub. No.: US2012/0170048A1

[1.18]. Peter de Groot, Middletown, CT (US); Michael Schroeder, East Hampton, CT (US). INTERFEROMETRIC HETERODYNE OPTICAL ENCODER SYSTEM United States Patent. 2012, Pub. No.: US2012/0194824 A1

[1.19]. Quinn, T. J., Mise en Pratique of the Definition of the Metre (1992). Metrologia, 1993/94. **30**: 523-541

[1.20]. International Technology Roadmap for Semiconductors. ITRS Reports: 2000 Update-2011 Edition 2012, www.itrs.net

[1.21]. HEIDENHAIN Brochure. Exposed Linear Encoders. March 2012

[1.22]. HEIDENHAIN Brochure. Linear Encoders for Numerically Controlled Machine Tools. August 2012

[1.23]. Product Catalog. MicroE Systems. 2012, Rev.B1-1

[1.24]. www.optra.com

[1.25]. RENISHAW. Non-contact position encoders. Issued 0707

[1.26]. Xingchun Chu, Haibao Lü and Shanghong Zhao. Research on long-range grating interferometry with nanometer resolution. Meas. Sci. Technol. 2008, 19: 017001

[1.27]. Marek Dobosz. High-resolution laser linear encoder with numerical error compensation. Opt. Eng. 1999, 38(6), 968-973

[1.28]. Chyan-Chyi Wu, Wen-Jong Wu, Zheng-Seng Pan, and Chih-Kung Lee. Laser linear encoder with both high fabrication and head-to-scale tolerances. APPLIED OPTICS, 2007 46 (16), 3169-3176

[1.29]. D Shin and B Kim. A laser interferometer encoder with two micromachined gratings generating phase-shifted quadrature. JOURNAL OF MICROMECHANICS AND MICROENGINEERING. 2011, 21: 085036

[1.30]. Fang Cheng and Kuang-Chao Fan. Linear diffraction grating interferometer with high alignment tolerance and high accuracy. APPLIED OPTICS, 2011, 50 (22): 4550-4556

[1.31]. Yanan Huang and Chia-Hsiang Menq. Design and development of a large range linear encoder with subnanometer resolution. REVIEW OF SCIENTIFIC INSTRUMENTS. 2006, 77: 105104

[1.32]. Chyan-Chyi Wu, Cheng-Chih Hsu, Ju-Yi Lee, and Cheng-Yang Liu. Optical Heterodyne Laser Encoder for In-plane Nanopositioning. Proc. of SPIE, 2008, 7063: 70631A

[1.33]. Ju-Yi Lee, Hui-Yi Chen, Cheng-Chih Hsu, Chyan-Chyi Wu. Optical heterodyne grating interferometry for displacement measurement with subnanometric resolution. Sensors and Actuators,2007, A 137: 185-191

[1.34]. Chyan-Chyi Wu, Cheng-Chih Hsu, Ju-Yi Lee, Hui-Yu Chen and Ching-Liang Dai. Optical heterodyne laser encoder with sub-nanometer resolution. Meas. Sci. Technol. 2008, 19: 045305

[1.35]. H L Hsieh, J Y Lee, W T Wu, J C Chen, R Deturche and G Lerondel. Quasi-common-optical-path heterodyne grating interferometer for displacement measurement. Meas. Sci. Technol., 2010, 21: 115304

[1.36]. Akihide Kimura, Wei Gao and Zeng Lijiang. Position and out-of-straightness measurement of a precision linear air-bearing

stage by using a two-degree-of-freedom linear encoder. Meas. Sci. Technol. 2010, 21: 054005

[1.37]. W. Gao, A. Kimura. A fast evaluation method for pitch deviation and out-of-flatness of a planar scale grating. CIRP Annals-Manufacturing Technology. 2010, 59: 505-508

2. Displacement laser interferometer

In principle, the main difference between displacement interferometers and interferometric encoders lies in the measurement standards. The measurement standard of an interferometer is the wavelength of its interfering light. And that of an interferometric encoder is the period of its scale grating. But both displacement interferometers and interferometric encoders employ the same detection techniques; so interferometeric encoders sometimes are also called as ‘grating interferometers’. Therefore it is necessary to introduce the displacement interferometers first.

2.1. Principle

The basis for most interferometers used in interferometric dimensional gages is the classical Michelson interferometer [2.1] which is schematically shown in Figure 2-1.

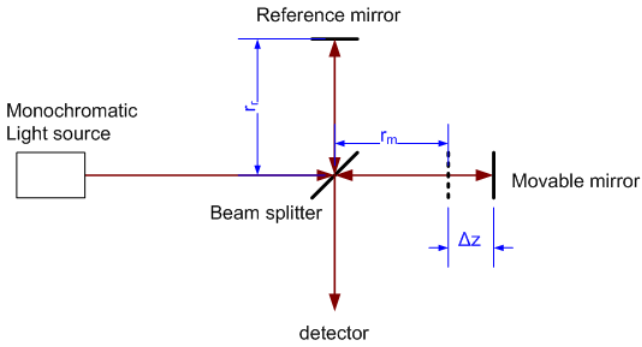

Figure 2-1. Schematic of the classical Michelson interferometer.

"Monochromatic light is directed at a semi-transparent mirror that acts as amplitude dividing beam splitter. Part of the light is transmitted toward a movable mirror and reflected by this mirror. The other part of the light is reflected at 90° towards a fixed mirror, reflected and recombined at the beam splitter, followed by the detection through detector. The electromagnetic waves propagating in reference and measurement arm can be represented as [2.2]:

$$\vec{E}_{ref} = E_r e^{i(\omega t + \vec{k} * \vec{r_r} - \phi_r)} \overrightarrow{e1} \quad (2.1)$$

$$\vec{E}_{meas} = E_m e^{i(\omega t + \vec{k} * \vec{r_m} - \phi_m)} \overrightarrow{e2} \quad (2.2)$$

With E_r and E_m the amplitude of the respective E-fields, ω the angular frequency, t the time, $\vec{k}$ the propagation vector, $\vec{r}$ the position vector, Φ_r and Φ_m the phase in reference and measurement arm. After recombination in the beam splitter, the electromagnetic field is the linear superposition of these waves. Assuming the propagation of the field in only one dimension, the irradiance at the detector becomes:

$$I = \epsilon_0 c \langle \overrightarrow{E^2} \rangle$$

$$= \epsilon_0 c(E_r^2 + E_m^2 + 2E_r E_m \cos\left(k(r_m - r_r) - (\phi_m - \phi_r)\right)) \quad (2.3)$$

Where ϵ_0 is the vacuum permittivity, c is the speed of light, k is the propagation constant ($k = 2\pi/\lambda$) and r_m is the traveled optical distance in the measurement arm and r_r is the traveled optical distance in the reference arm. The constant $\epsilon_0 c$ will be omitted in further calculations for convenience. If the waves are initially in phase ($\Phi_r = \Phi_m$), the cosine term depends on the optical path length difference between reference and measurement arm. This is the case for a coherent light source. If the two beams are also of equal amplitude, the irradiance is:

$$I = 2I_0(1 + \cos\left(\frac{2\pi}{\lambda}(r_m - r_r)\right)) \quad (2.4)$$

When the measurement mirror is displaced over a distance Δz while the reference mirror remains fixed, the optical path length difference changes 2nΔz, with n the refractive index of the medium through which the light travels. The factor 2 is due to the fact that this distance is traveled twice by the light. Then the detected signal can be expressed as following:

$$I = 2I_0(1 + \cos\left(\frac{2\pi}{\lambda}(2n\Delta z)\right)) \quad (2.5)$$

If the wavelength of the light source is known, the displacement Δz can be calculated from the change in intensity on the detector. From this it can also be seen that it is a relative measurement, only displacement can be measured, not distance."[1]

[1] Cited from Reference [2.2] (pages: 2-4)

2.2. Frequency. stabilized lasers

The current definition of meter is as follow:

The metre is the length of the path travelled by light in vacuum during a time interval of 1/299 792 458 of a second [2.3].

For interferometers, in order to attain the best possible accuracy, great care must be taken to ensure the highest wavelength stability of the light source [2.4]. A laser can be used as a standard for dimensional metrology only if its wavelength or frequency is stabilized e.g. to suitable reference frequencies of atoms, molecules or ions. Depending on the intended application, the construction of frequency or wavelength standards follows two different philosophies. If simplicity of use and operation is the primary goal then one starts with an easy-to-handle laser whose frequency can be tuned only in a very limited range. Examples include the well known HeNe gas laser or Nd:YAG lasers. In this case, only absorption lines coinciding with the narrow emission ranges of these lasers can be selected as reference lines for the stabilization. The second philosophy avoids this restriction to accidental coincidences between laser lines and absorption lines by choosing an 'ideal' absorption line. The higher accuracy achievable with this approach, in general has to be paid for by the use of widely tunable, coherent light sources like dye lasers, diode lasers, optical parametric oscillators and the implementation of extra methods to operate these sources in single mode and stable conditions despite of the wide tuning range [2.5].

2.3. Refractive index of the air

The measurement standard of a displacement interferometer which is operated in ambient air is given by $\lambda_A = \lambda_V/n$, where λ_A is the wavelength of the laser source in air, λ_V is the wavelength in vacuum and n is the refractive index of air. The refractive index depends on wavelength, pressure, temperature and the air composition. The following values give an approximation of the influence of the main environmental parameters on the refractive index [2.5]:

$$\frac{\Delta n}{\Delta T} \approx -10^{-6} K^{-1}$$

$$\frac{\Delta n}{\Delta p} \approx 2.7*10^{-9} Pa^{-1}$$

$$\frac{\Delta n}{\Delta h_r} \approx -10^{-8} (\%)^{-1}$$

$$\frac{\Delta n}{\Delta CO_2} \approx 1.5*10^{-10} ppm^{-1}$$

Where, ΔT, Δp, Δh_r and ΔCO_2 are the deviations of temperature, pressure, humidity and the CO_2 content.

There are two main principles used to determine the refractive index. The first principle is the indirect determination through the measurement of above parameters and calculation of n using Edlen's equation [2.6] and its improved versions [2.7-2.10]. The second principle is the direct interferometric measurement of n using a refractometer [2.5].

2.4. Homodyne displacement interferometer

A homodyne interferometer employs a single-frequency laser source and normally quadrature detection technique. An example is shown in Figure 2-2 [2.11]. The single-frequency laser beam with 45° linear polarization is split into two sub-beams by a polarization beam splitter (PBS): one sub-beam is directed to and reflected back by the fixed reference retroreflector, another one is directed to and reflected back by the measurement retroreflector. The detection unit consists of a quarter wave plate (λ/4), a half wave plate (λ/2), a beam splitter (BS), two PBSs and four photodetectors (PD). The interference signals detected by the four photodetectors have the phases of 0°, 90°, 180° and 270° respectively. Two signals with a phase difference of 90° are obtained by subtracting the signal with phase of 180° from the signal of 0° and the signal with phase 270° from the signal of 90° as shown in Figure 2-3. Because the offsets are common values for four photodetectors, they can be almost removed by the subtracting. The direction of the movement of the measurement retro-reflector can now be determined at the zero crossing of the interference signal using the sign of the other signal as shown in Figure 2-4 [2.12]. The integer part of the signal phase can be calculated through zero-crossing. And the fractional part of the signal phase can be determined from the intensities of the 0° and the 90° signal with equation (2.6).

$$\Phi = \arctan(I_0/I_{90}) \qquad (2.6)$$

Where, Φ is the fractional part of the signal phase; I_0 and I_{90} are the intensities of 0° and 90° signals respectively [2.12].

In principle, when there is no movement, there is also no measurement signal in the homodyne displacement interferometer. Therefore homodyne interferometers also are known as DC interferometers. But compared to heterodyne interferometers, homodyne interferometers don't have a theoretical limitation of the moving speed of the measurand [2.4].

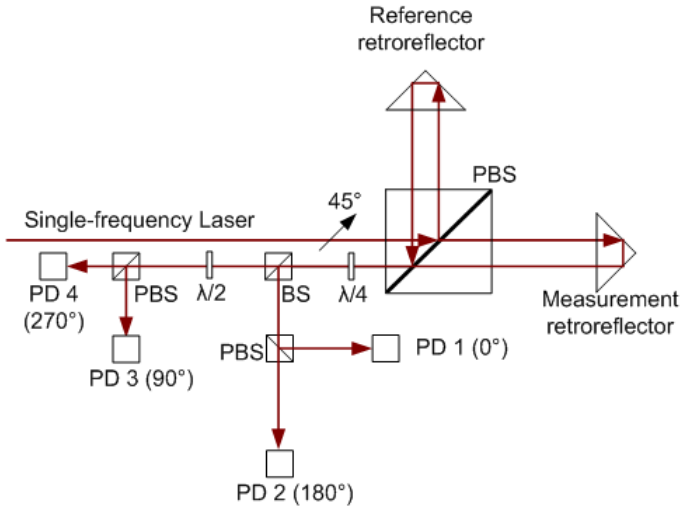

Figure 2-2. Schematic of a homodyne displacement interferometer; PBS is polarization beam splitter, BS is beam splitter, λ/2 is half wave plate, λ/4 is quarter wave plate, P is polarizer, PD is photodetector.

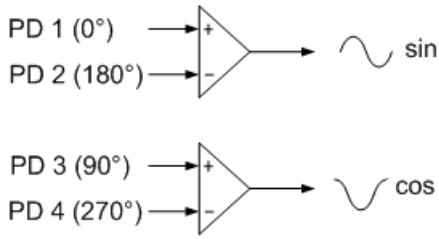

Figure 2-3. Signal processing diagram of the four quadrature signals.

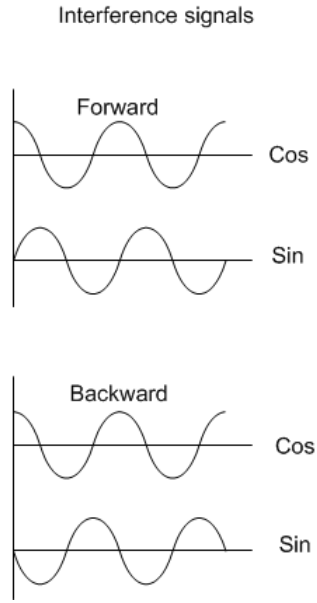

Figure 2-4. Schematic of the movement-direction determination.

2.5. Heterodyne displacement interferometer

One example of heterodyne displacement interferometers is shown in Figure 2-5 [2.2]. The double-frequency laser emits two frequencies (f_1 and f_2) laser light. Light components f_1 and f_2 have linear polarization with orthogonal polarization directions to each other. The beat frequency $\Delta f = f_2 - f_1$ should be detectable for the detection and signal processing electronics. Normally Δf is in the MHz range, which can be generated through Zeeman effect and acousto-optic modulation among others. “The electromagnetic fields of those two light components can be represented by:

$$\vec{E}_1 = E_{01} e^{i(2\pi f_1 t + \phi_{01})} \vec{e_1} \quad (2.7)$$

$$\vec{E}_2 = E_{02} e^{i(2\pi f_2 t + \phi_{02})} \vec{e_2} \quad (2.8)$$

Where E_{01} and E_{02} are the amplitudes and Φ_{01} and Φ_{02} represent the initial phase of the electromagnetic fields.

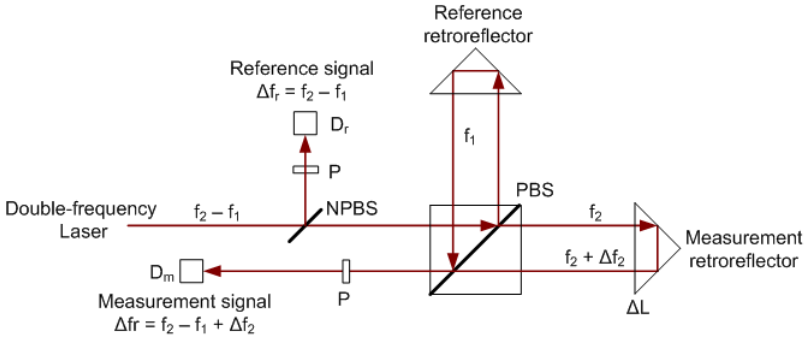

Figure 2-5. Schematic of a heterodyne displacement interferometer; PBS is polarization beam splitter, NPBS is non-polarization beam splitter, P is polarizer, D is detector.

The detected reference signal I_r is given by:

$$I_r = 2E_{01}E_{02} \cos(2\pi(f_2 - f_1)t + (\Phi_{02} - \Phi_{01})) \quad (2.9)$$

As can be seen from this equation, the heterodyne interferometer works with a carrier frequency Δf_r, therefore it is called an AC interferometer. The measurement signal can be represented by:

$$I_m = 2E_{01}E_{02} \cos(2\pi(f_2 - f_1)t + (\Phi_{02} - \Phi_{01}) + (\Phi_{meas} - \Phi_{ref})) \quad (2.10)$$

$$\Phi_{meas} - \Phi_{ref} = \Delta\Phi + \Phi_{0m} - \Phi_{0r} \quad (2.11)$$

Where, $\Phi_{meas} - \Phi_{ref}$ is the phase difference between the measurement arm and the reference arm. $\Delta\Phi$ is the phase resulting from the

moving of the retroreflector. Φ_{0m} and Φ_{0r} are the initial phases of the measurement arm and the reference arm respectively. The measurement retroreflector is attached to the measurand; as it moves with a velocity v, a Doppler shift is generated for frequency f_2:

$$\Delta f = 2v*n*f_2/c \qquad (2.12)$$

Where, n is the refractive index of air which this interferometer works in; c is the speed of light in vacuum. Equation (2.12) also indicates that the maximum traveling speed of the retroreflector is limited by the beat frequency of the laser source. The phase change resulting from the Doppler shift is:

$$\Delta\phi = \int_{t1}^{t2} 2\pi\Delta f dt = \int_{t1}^{t2} 2\pi \frac{2vnf_2}{c} dt = 4\pi \frac{nf_2}{c} \int_{t1}^{t2} v dt = 4\pi \frac{f_2}{c} \Delta L \qquad (2.13)$$

Here ΔL is the displacement of the retroreflector. Therefore by measuring the phase change between reference (2.9) and measurement (2.10) signals, the displacement of the retroreflector can be determined by:

$$\Delta L = \Delta\Phi\lambda_2/(4\pi n) \qquad (2.14)$$

Here, λ_2 is the vacuum wavelength of the light component whose frequency is f_2."[2]

References

[2] Based on Reference [2.2] (pages: 5-7)

[2.1]. W. R. Steel, Interferometry, 2nd ed., (Cambridge studies in modern optics), Cambridge, U.K.: Cambridge University Press, 1985

[2.2]. Suzanne J. A. G. Cosijns. Displacement laser interferometry with sub-nanometer uncertainty. 2004 Dissertation, Technische Universiteit Eindhoven

[2.3]. Resolution 1 of the 17th meeting of the CGPM (1983). Metrologia, 1984, 20(1), 25

[2.4]. John G. Webster et al. THE MEASUREMENT, INSTRUMENTATION, AND SENSORS HANDBOOK. ISBN 3-540-64830-5

[2.5]. Edited by Julian D. C. Jones and Colin E. Webb. Handbook of Laser Technology and Applications. Taylor & Francis, 2004, ISBN: 978-0-7503-0607-2

[2.6]. Edlen, B., The refractive index of air. Metrologia, 1966, 2:71-80

[2.7]. Muijlwijk, R., Update of the Edlen formulae for refractive index of air. Metrologia, 1988, 25:189

[2.8]. Birch, K. P. and M. J. Downs, Correction to the updated Edlen Equation for the Refractive index of Air. Metrologia, 1993, 30: 155-162

[2.9]. Birch, K. P. and M. J. Downs. An Updated Edlen Equation for the Refractive Index of Air. Metrologia, 1994, 31:315-316

[2.10]. Bönsch, G. and E. Potulski. Measurement of the refractive index of air and comparison with modified Edlen's formula. Metrologia, 1998, 38:133-139

[2.11]. TaeBong Eom, JongYun Kim and Kyuwon Jeong. The dynamic compensation of nonlinearity in a homodyne laser interferometer. Measurement Science and Technology, 2001, 12: 1734-1738

[2.12]. Colin E. Webb, Julian D. C. Jones. Handbook of Laser Technology and Applications, Volume 3. Philadelphia, 2004, ISBN: 0750309660

3. Interferometric encoder

3.1. History

Optical encoders evolved from contact encoders [3.1]. Up to now, from my searching, the first formal publication about the optical encoder was made by Follingstad, H. G. from Bell Telephone Laboratories [3.2]. This chronogram can also be confirmed through the information provided by HEIDENHAIN [3.3].

3.2. Principle of linear optical encoder

A linear optical encoder has two basic parts: a grating scale and an encoder head. When there is relative displacement between these two parts, detectable information will be generated correspondingly. There are basically three techniques to generate such detectable information: geometric masking, Moire effects and laser interference.

3.2.1. Geometric masking

As shown in Figure 3-1, the simplest form of linear optical encoder based on geometric masking is composed of four basic parts: light source (LS), optics unit, grating scale and detection unit. LS normally is a lamp or LED (Light-emitting diode). The scale grating here is an amplitude grating which modulates the amplitude of the incident light. The collected emitting light is formed into certain profile by the optics unit before it reaches the grating scale. After interacting with the grating scale, the transmission light is detected by the detection unit. When there is relative movement between the grating scale and the rest units, the intensity of the transmission light will be correspondingly modulated by this relative movement before being detected and processed by the detection unit. Then the relative movement can be attained.

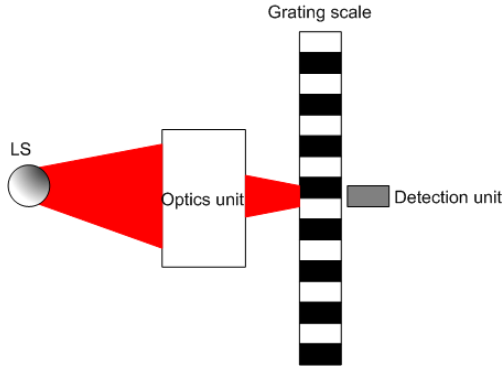

Figure 3-1. Schematic of the simplest encoder based on geometric masking; LS is light source.

Limited by the diffraction effect, the period of this amplitude grating is relatively large. Therefore the linear encoders based on geometric masking are only used for coarse measurement.

3.2.2. Moire effect

A simplest Moire-effect-based linear encoder consists of a grating scale, index grating, light source, optics unit and detection unit, as shown in Figure 3-2.

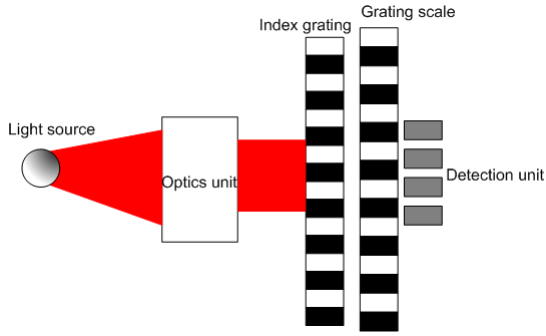

Figure 3-2. Schematic of the simplest encoder based on Moire effect.

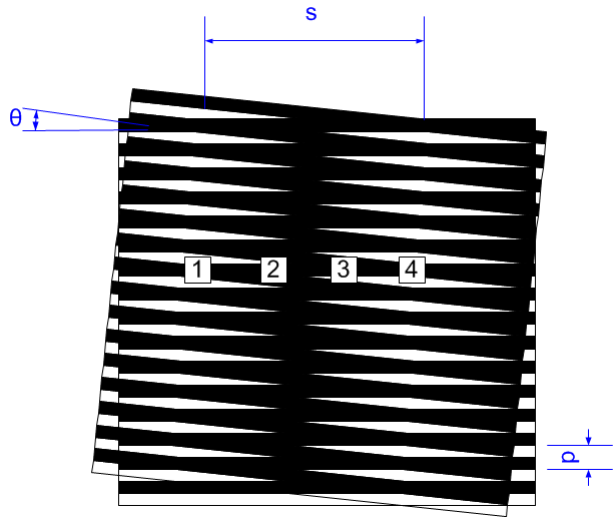

Figure 3-3. Schematic of Moire effect; 1, 2, 3 and 4 are the schematic positions of the detector elements.

Figure 3-3 shows one form of Moire fringes generated by the index grating and the grating scale. The grating scale and the index grating have the same pitch p; these two gratings are parallel but with a relative rotation angle of θ. The fringe spacing s can be expressed as [3-4]:

$$s = p/ [2\sin (\theta/2)] \quad (3.1)$$

Relatively to the index grating, as the grating scale moves by one grating pitch perpendicular to its lines, the moiré fringes move by one fringe period. Normally θ is a small value which will result an actual optical amplification factor of 1/ [2sin (θ/2)] for the period of the grating scale. This will enhance the optical resolutions of moiré-effect-based encoders compared to the geometric-masking-based encoders. But the period of the grating scale is still limited by the diffraction effect, which will eventually limit the resolutions of this kind of encoder. Moreover, during working, the accuracy of a Morie-effect-based encoder is very sensitive to the angular deviations between its grating scale and index grating, especially the fluctuation of θ.

3.2.3. Laser interference

An encoder based on laser interference is more commonly called as “optical interferometric encoder” or simplified as ‘interferometric encoder’ which this thesis is focused on. In current encoder family, the interferometric encoder can achieve the highest level of performance. In principle, both interferometric encoders and the displacement interferometers are based on the laser interference. As mentioned at the beginning of chapter 2, the main difference between them is that interferometric encoders use the period of the grating scale as the measurement standard but the displacement

interferometers use the wavelength of the laser. Just like displacement interferometers, interferometric encoders also can be separated into homodyne interferometric encoders and heterodyne ones. As examples, Figure 3-4 shows the schematics of a homodyne interferometric encoder and a heterodyne one.

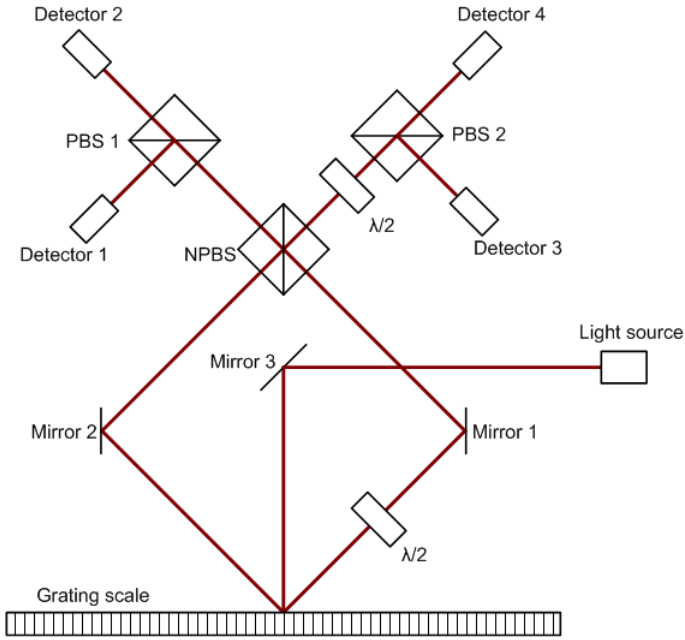

(a)

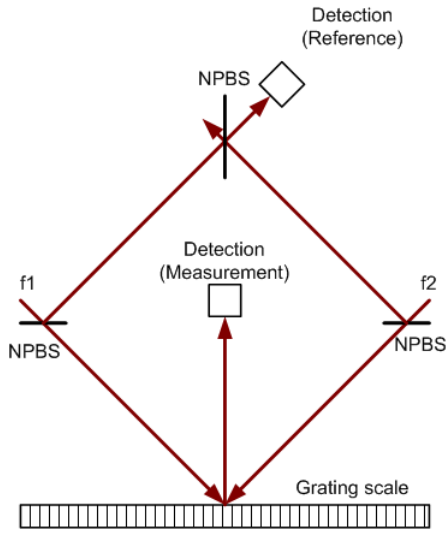

(b)

Figure 3-4. (a) Schematic of a homodyne encoder; (b) schematic of a heterodyne encoder; NPBS is non-polarization beam splitter, PBS is polarization beam splitter, $\lambda/2$ is half wave plate.

3.2.4. Detection and signal processing

For an optical interferometric encoder, to get the measured displacement information from its optical signal, basically the following functional stages shown in Figure 3-5 are needed:

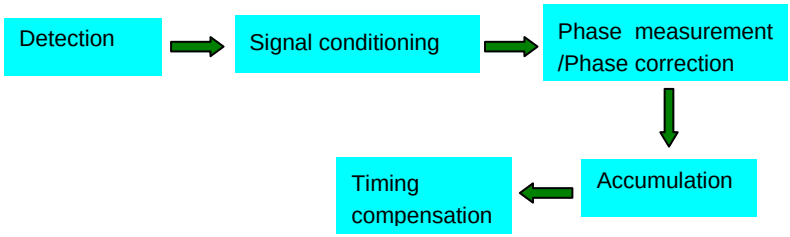

Figure 3-5. Block diagram of the signal processing of an optical interferometric encoder.

3.2.4.1. Detection

Detection stage is used to convert the optical signal to electrical current signal. Normally it is realized by certain number of photodiodes or photodiode arrays. Concerning the response speed, in most cases the photodiodes are PIN type photodiodes.

3.2.4.2. Signal conditioning

For all signal processing schemes of an optical encoder, a function of transimpedance amplification is indispensable. Other functions like voltage shifting, analog to digital conversion, normalization and filtering will also be included in this stage for some signal processing schemes. For example, voltage shifting and analog to digital conversion are necessary in this stage for those schemes which are based on digital phase meters.

3.2.4.3. Phase measurement/ Phase correction

This stage is the heart of the signal processing. The correlation between the periodicity of the grating scale and the relative

displacement leads to the generation of a corresponding periodic voltage signal after the detection and signal conditioning. To determine the displacement of the measurand, the phase of the periodic voltage signal needs to be measured in this stage. There are different techniques to measure the phase; some of the frequently used ones are listed in the following:

Zero-crossing: As an example, the phase measurement technique based on zero-crossing employed by ZYGO AXIOM 2/20 [3.5] is shown in Figure 3-6.

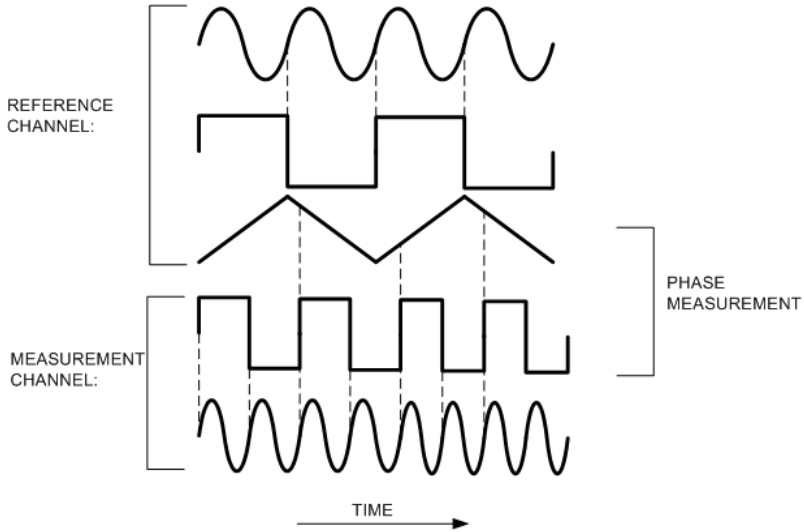

Figure 3-6. Schematic of phase measuring technique of ZYGO AXIOM 2/20 [3.5].

Figure 3-6 shows how the phase difference between measurement channel and reference channel is measured. The stable 20 MHz sinusoidal electrical reference signal and the sinusoidal optical interference measurement signal are each converted into square

waves of half the frequency. The reference square wave is further integrated to produce a triangular wave. The triangular wave is sampled and digitized by an analog-to-digital converter at each positive transition of the measurement square wave. Its value is then compared to the previous reading and any difference is added to an accumulator.

Fast Fourier Transform: "In the fast Fourier transform (FFT) method, the digital signal samples are Fourier transformed with an FFT. If the signal is sinusoidal, the initial phase is estimated as that value of the phase where the Fourier transform is maximized. The frequency of the signal is estimated as that value of frequency where the Fourier transform is maximized. Once measurements of the frequency f and initial phase Φ_0 have been obtained, the phase Φ at any point in time t can be calculated according to [3.6]:

$$\Phi = 2\pi ft + \Phi_0 \qquad (3.2)$$

"[3] One of the applications of this technique in optical encoder was reported by Xingchun Chu, *et al.* [3.7].

Counter + interpolation: In this technique, the integer part of the signal periods is counted by a counter which is a commercially available module; the interpolation of the fractional part of the signal period is performed in a data-processing unit such as DSP(Digital Signal Processor), FPGA(Field-Programmable Gate Array) and CPU(Central Processing Unit) and so on. This technique is adopted by HEINDENHAIN [3.8] and RENISHAW [3.9], as shown in Figure 3-7 and Figure 3-8.

[3] Cited from Reference [3.6] (chapter 5, page: 12)

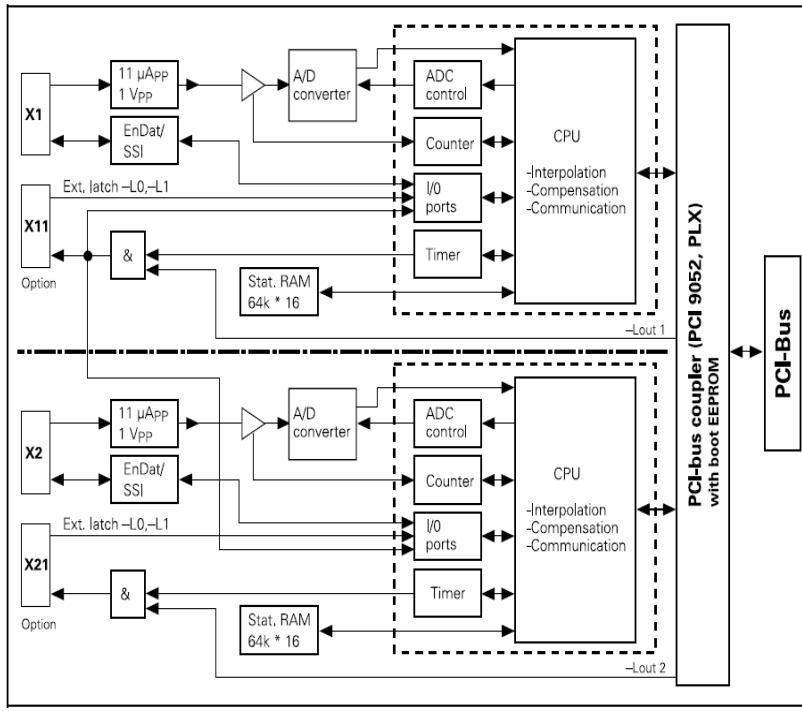

Figure 3-7. Basic circuit diagram of HEIDENHAIN IK 220 [3.8].

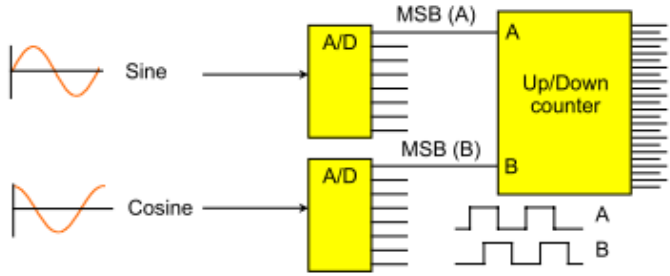

(a)

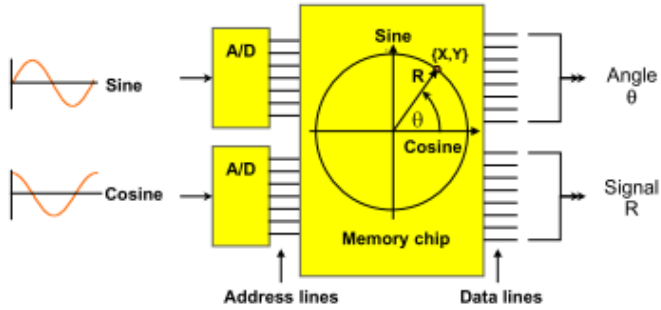

(b)

Figure 3-8. (a) Schematic of a RENISHAW counting circuit; (b) schematic of a RENISHAW interpolation and signal strength monitoring circuit [3.9].

Digital demodulation: In this technique, after the digitalization of the detected signals, all the phase measurement is implemented in a digital data process unit such as DSP, FPGA and CPU. There are a number of reported optical encoders based on this technique [3.27-3.30, 3.43]; in those reports, all the phase measurements are based on lock-in principle.

Phase-Locked Loops: "If the signal frequency does change substantially during measurement, one means to estimate the phase of the signal is to use a phase-locked loop (PLL). In this case, the signal $s(t) = A*\sin(\omega t + \varphi(t))$ can be thought of as a constant frequency component $A*\sin(\omega t)$, which is phase modulated by a time-varying phase component $\varphi(t)$. The problem then reduces largely to one of demodulating a phase-modulated (PM) signal. A PLL can be used to form an estimate of the 'phase-modulating' component $\hat{\varphi}(t)$ and the overall phase of the signal φ_{oa} can be estimated according to [3.6]:

$$\varphi_{oa}(t) = \omega t + \hat{}\varphi(t) \qquad (3.3)$$

"[4] Yanan Huang and Chia-Hsiang Menq reported an encoder which was based on the PLL technique [3.10]. And encoders from NanoWave are also based on this technique [3.11].

Vernier principle: This kind of meter emulates a Vernier caliper and inherits its characteristics. Phase difference may be measured in any period of the measured signals. In the basic theory, two phase-locked-loop circuits are used as frequency multipliers which divide each period of the input signals into multiple equal time slots, thereby emulating the divisions of space inscribed on the scales of a caliper. A simple ''pseudophase detector'' made of a D-type flip–flop is used to compare the location of the time slots on both of the scales, just as we use the Vernier caliper [3.12].

The most widely used phase-correction algorithm is invented by Heydemann [3.13]. It uses ellipse fitting to calculate the real fractional phase. The original Heydemann correction is presented with zero-crossing-phase-measurement technique. Chien-ming Wu further developed this algorithm for the digital interpolation [3.14]. Although Chien-ming Wu presented this further-developed Heydemann correction algorithm for homodyne detection, actually this algorithm is suitable for all the fractional phase interpolation which is based on the calculation of the arctangent of two quadrature signals (sine and cosine), no matter in homodyne detection or heterodyne detection.

[4] Cited from Reference [3.6] (chapter 5, page: 13)

3.3. Grating

The interaction of light with matter can take many forms. Among them, absorption, reflection and diffraction are utilized by optical encoders. Based on the interaction forms, the grating scales of the optical encoders can be put into two groups: diffraction gratings and non-diffraction gratings (also known as *intensity gratings* in some literature.). Diffraction gratings, which change the phase of the interacted light, are used as grating scales of interferometric encoders. And the non-diffraction gratings, which only change the intensity of the interacted light, are employed as grating scales by the optical encoders based on geometric masking and moiré effect. In the following, only the diffraction gratings will be briefly introduced.

In this thesis, the sign convention of the incidence and diffraction beams is following: angles of incidence and diffraction are measured from the grating normal to the beam, positive in the counterclockwise direction and negative in the clockwise direction.

“An illustration of grating diffraction, using wave fronts (surfaces of constant phase), is shown in Figure 3-9 [3.15]. The geometrical path difference between light from adjacent grooves is seen to be d*sin (α) + d*sin (β), in which d is the pitch or period of the grating. Since $\beta<0$, the latter term is actually negative. The principle of interference dictates that only when this difference equals the wavelength λ of the light, or some integral multiple thereof, will the light from adjacent grooves be in phase (leading to constructive interference). At all other angles β, there will be some measure of destructive

interference between the wavelets originating from the groove facets. These relationships are expressed by the grating equation:

$$m^* \lambda = d^*(\sin(\alpha) + \sin(\beta)) \quad (3.4)$$

Here m is the diffraction order, which is an integer. For a particular wavelength λ, all values of m for which $|m^* \lambda/d| < 2$ correspond to physically realizable diffraction orders.

It is sometimes convenient to write the grating equation as

$$G^* m^* \lambda = \sin(\alpha) + \sin(\beta) \quad (3.5)$$

Where G = 1/d is the groove frequency or groove density, more commonly called ‘grooves per millimeter’.

Equation (3.4) and its equivalent equation (3.5) are the common forms of the grating equation, but their validity is restricted to cases in which the incident and diffracted rays are perpendicular to the grooves, which is called classical (or in-plane) diffraction. If the incident light beam is not perpendicular to the grooves, though, the grating equation must be modified:

$$G^* m^* \lambda = \cos(\varepsilon)^*(\sin(\alpha) + \sin(\beta)) \quad (3.6)$$

Here ε is the angle between the incident light path and the plane perpendicular to the grooves at the grating center. In geometries for which $\varepsilon \neq 0$, the diffracted beams lie on a cone rather than in a plane, so such cases are termed conical diffraction.

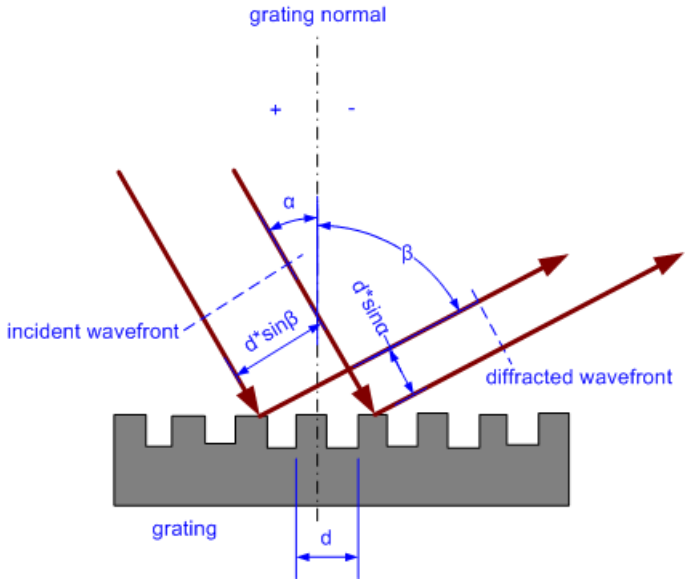

Figure 3-9. Geometry of diffraction, for planar wavefronts.

A special but common case is that in which the light is diffracted back toward the direction from which it came (i.e., α = β); this is called the Littrow configuration, for which the grating equation becomes

$$m^* \lambda = 2^*d^*\sin(\alpha) \text{ , in Littrow} \qquad (3.7)$$

There are four common methods to manufacture a grating: ruling with ruling machine, interference (so called Holographic method), lithography and replication.

Ruling: The first diffraction gratings made for commercial use were mechanically ruled, manufactured by burnishing grooves individually with a diamond tool against a thin coating of evaporated metal applied to a plane or concave surface [3.15].

Interference: Since the late 1960s, a method distinct from mechanical ruling has also been used to manufacture diffraction gratings. This method involves the photographic recording of a stationary interference fringe field. Such interference gratings more commonly are known as holographic gratings [3.15].

Replication: the process for making replica gratings results in a grating whose grooves are formed in a very thin layer of resin that adhere strongly to the surface of the substrate material. The optical surface of a reflection replica is usually coated with aluminum, but gold or platinum is recommended for greater diffracted energy in certain spectral regions. Transmission gratings have no reflective coating [3.15]"[5].

Lithography: Gratings also can be produced through the process which is used to manufacture the IC (integrated circuit).

3.4. Measurement uncertainty of interferometric encoder

Following the guide of JCGM (Joint Committee for Guides in Metrology), in this thesis, instead of accuracy or precision, measurement uncertainty is adopted to indicate corresponding characteristics of the interferometric encoder. According to JCGM, measurement uncertainty is defined as:

Parameter, associated with the result of a measurement that characterizes the dispersion of the values that could reasonably be

[5] Based on Reference [3.15] (pages: 17-19, 38, 43, 55)

attributed to the measurand. NOTE 1: the parameter may be, for example, a standard deviation (or a given multiple of it), or the half-width of an interval having a stated level of confidence [3.16].

As listed in Table 3-1, there are varieties of contributors which will lead to measurement uncertainty of an interferometric encoder.

Table 3-1. Contributors of measurement uncertainty of an interferometric encoder.

Group	Contributor	Feature
Environmental contributors	Temperature fluctuation	random
	Pressure fluctuation	random
	Other factors which will result in the fluctuation of the refractive index of the ambient air.	random
	Vibration	random
Optical contributors	Multi-reflections	systematic
	Polarization mixing	systematic
	Optical path difference between two interfering beams	Random (Taking effect through correlation with deviations of the wavelength and refractive index)

	Imperfection and contaminations of the scale grating	Systematic As-built
Photonic contributors	Wavelength deviation	random
	Power fluctuation	random
	Laser pointing deviation	random
	Laser polarization deviation	random
Electronic contributors	Noise	random
	Quantization error	random
	Unequal gain, DC shift between different channels	systematic
	Data age*	systematic
Alignment contributors	Cosine error	systematic
	Abbe error	Random/systematic
	Deviations of angular-and-linear-relative-position between the encoder head and the scale grating in the non-measurement direction.	Random (take effect through correlation with the relevant sensitivities of the encoder)

* Two forms of inherent uncertainty are called fixed delay and variable delay. Fixed delay arises from differences in cable lengths, optical

path lengths, photoelectric detector delay, and phase meter offsets in interferometry systems, whereas circuit delay, i.e., group delay, (which varies with signal frequency) give rise to variable delay. The effects of these delays create differences in the data age of the interferometrically measured values, i.e., the elapsed time between the event representing the position measurement, and when the position data is available to the user [3.17].

For a specific interferometric encoder, it is not necessary that all the listed contributors will take effect. It depends on the design of the encoder itself. Better design will reduce more influence of the measurement-uncertainty contributors.

3.5. Displacement laser interferometers versus interferometric encoders

In comparison with each other, both displacement laser interferometers and interferometric encoders have their intrinsic pros and cons, as shown in Table 3-2.

Table 3-2. Displacement laser interferometers versus interferometric encoders.

	Displacement laser interferometer	**Interferometric encoder**
Being directly traceable to the definition of SI meter	Possible 	Not possible

Meeting Abbe principle	Easily 	Not so easily
Influence of the topography of the measurement mirror (for interferometer) and the imperfection and contaminations of the scale grating (encoder)	Have	Have
Requirement on the frequency stabilization of the light source	Strict	Not so strict 
Requirement on the coherence length of the light source	Strict	Not so strict 
Sensitivities to the deviation of the refractive index of the ambient air	High	Non so high 

For the majority of the industrial applications, direct traceability to the definition of SI meter is not relevant. Currently for the displacement measurements which require measurement ranges of hundreds of millimeters and measurement uncertainties in the order of a few nanometers or even below, displacement laser interferometers and interferometric encoders are the dominating solutions. But compared to interferometric encoders, to achieve nanometer order or even lower measurement uncertainties, displacement laser interferometers

require much stricter environment control if not vacuum. Therefore interferometric encoders are getting more and more preferable.

3.6. Recent development of the interferometric encoders

In this section, the recent development of the interferometric encoders is separated into three following sub-sections, according to the types of the interferometric encoders. In addition, concerning the big number of involved prior works, only brief introductions of them are given here. Through reviewing these prior works, the pre-stated relevant conclusion in the section 1.2 can be verified.

3.6.1. Homodyne interferometric encoder

Marek Dobosz reported an interferometric encoder with resolution of 10 nm and nonlinearity of less than 0.1 μm over 48 mm measuring range [3.18]. Chyan-chyi Wu *et al* presented an interferometric encoder with measurement accuracy of 37.3 nm [3.19]. An interferometric encoder with measurement precision of less than 10 nm was reported by Xingchun Chu *et at* [3.7]. This encoder was based on a transmission scale grating. And an improved FFT algorithm was used to extract the phase information of the detected interference fringe pattern. An ‘interferometric encoder’ based on only two gratings was put forwarded by D Shin and B Kim [3.20]. Its quadrature signal was generated through the phase difference of two gratings which were manufactured on the same substrate. The problem of this report is that: although the authors called this system

“a laser interferometer encoder”, actually it was a displacement interferometer, simply because its measurement standard was still the wavelength of the laser instead of the period of the grating. Two gratings were used only to get the quadrature signals in that system. One of a series of works upon the interferometric encoder developed by Kuang-Chao Fan’s group was presented by Fang Cheng [3.21]. This reported interferometric encoder had a repeatability of 15 nm within 15 mm travel length.

Beside the aforementioned papers, there are also a big number of patents about the homodyne interferometric encoders. Concerning the number of patents and the nature of the patent in general, in this dissertation, only the reference information of some of them are provided here [3.22-3.26].

3.6.2. Heterodyne interferometric encoder

Chyan-Chyi Wu *et al* used two measurement channels to get double optical subdivision. The beat frequency of this encoder is 1 KHz. And the phase evaluation was based on the lock-in principle. The achieved measurement uncertainty was less than 5 nm [3.27]. Ju-Yi Lee *et al* reported a heterodyne interferometric encoder with resolution of 0.2 nm. In this report, a transmission grating was employed as the grating scale; the detection scheme was also based on lock-in principle [3.28]. In 2008, Chyan-Chyi Wu *et al.* reported another heterodyne interferometric encoder with sub-nanometer resolution [3.29]. It was based on two sets of conjugate optics to achieve quasi-common-path configuration between two interfering beams of its measurement channel. A design which is more close to

the real common-path configuration was presented by H L Hsieh [3.30]. In this encoder, the quasi-common path was realized through the fact that: different parts of a converged beam have different diffraction behavior through the transmission scale grating but with overlapped area between the different diffraction orders of the aforementioned different parts of the converged incident beam. This encoder had resolution of better than 3 nm and a system stability of less than 14nm over one hour (which was the change of the linear fitting of the raw data. According to the relevant figure (Figure 8 of reference [3.30]), the peak-to-peak value of that stability should be around 50 nm.

Similar to the situation of homodyne interferometric, there is also a big quantity of patents about heterodyne interferometric encoders. Some of them are listed in the reference [3.31-3.36].

In the dimensional metrology field, related companies are the dominating players and technical powerhouses. For a company, patent is the main form of scientific publication. The distribution and trend of patents normally will indicate the direction of technical evolution. The current situation in the dimensional metrology field is that: in addition to the traditional encoder producers like HEIDENHAIN and so on, ZYGO which previously focuses on displacement interferometers and ASML which is the leading lithography machine tools provider, also turn attention to the interferometric encoders [3.32-3.42].

3.6.3. Multi-dimensional interferometric encoder

In this thesis, only the multi-dimensional interferometric encoders, which can meet all the following three criteria at the same time, will be discussed:

(1) The scale grating is a one-dimensional grating;
(2) The measurement standard of one basic measurement axis is the period of the grating, and for the additional axis(axes), at least part of the measurement standard(s) is (are) the period(s) of the grating(s);
(3) Each has only one encoder head; moreover, the encoder head is not any form of combination from a number of single encoder heads which can theoretically work independently.

Those so called “multi-dimensional interferometric encoders” or “multi-degree-of-freedom encoders”, which cannot meet the three criteria at the same time, normally are the combination of one-dimension encoder(s), displacement interferometer(s) or other kinds of displacement sensor(s). Theoretically, they don’t have too much of technical difference from the normal one-dimensional encoders.

Therefore, following these criteria, there is no commercially available multi-dimensional interferometric encoder product yet. Also up to now, according to my knowledge, there is only one paper in which a real two-dimensional encoder was presented [3.43], which is a prior publication upon part of this thesis work. Even for the reported encoder [3.44, 3.45], it is also not a real multi-dimensional

interferometric encoder since only one of its two measurement axes employ the period of the grating as measurement standard. Actually it is a combination of a one-dimensional encoder and a displacement interferometer. But the principle of this reported two-dimensional encoder had some technical significance; it was not a simply combination from common known solutions. However from my point of view, this solution also has a serious intrinsic drawback: its signal contrast should be strongly sensitive to the angular deviation of the scale grating with respect to its reference grating, which means the angular deviation of its scale grating should be strictly controlled during the movement of its scale grating, otherwise this two-dimensional encoder at least cannot work properly.

Up to now there is only one found patent [3.33] which presents a real two-dimensional interferometric encoder. For patent [3.46], the described multi-dimensional encoders unfortunately are also a combination of one-dimensional encoder(s) and interferometer. But just like the publications [3.44, 3.45], this publication also presents some technical innovation, therefore I also want mention it in this thesis.

References

[3.1.] David S. Nyce. Linear Position Sensors: Theory and Application. John Wiley & Sons, Inc., ISBN 0-471-23326-9

[3.2.] Follingstad, H.G. An Optical Position Encoder and Digit Register. Proceedings of the IRE, 1952, 40(11), 1573-1583

[3.3.] HEIDENHAIN. Milestones of Encoders. www. Heidenhain.de. 2012

[3.4.] John G. Webster, et al. THE HANDBOOK MEASUREMENT, INSTRUMENTATION, AND SENSORS. ISBN 3-540-64830-5

[3.5.] ZYGO AXIOM 2/20 LASER MEASUREMENT SYSTEM Operation and Reference Manual OMP-0220. April, 1988

[3.6.] John G. Webster, et al. ELECTRICAL MEASUREMENT, SIGNAL PROCESSING, and DISPLAYS. ISBN 0-8493-1733-9

[3.7.] Xingchun Chu, Haibao Lü and Shanghong Zhao. Research on long-range grating interferometry with nanometer resolution. Meas. Sci. Technol. 2008, 19: 017001

[3.8.] Product Information IK 220 Interpolation and Counter Card. HEIDENHAIN, 2006

[3.9.] Mark Chapman. Heterodyne and homodyne interferometry. RENISHAW, 2002

[3.10.] Yanan Huang and Chia-Hsiang Menq. Design and development of a large range linear encoder with subnanometer resolution. Rev. Sci. Instrum. 2006, 77: 105104

[3.11.] Susumu MAKINOUCHI, Toru IMAI, Akihiro WATANABE JinHock ONG and Tetsuo OHARA. Introduction of SPPE-1000 Scanning interference Optical Encoder. www.nanowave.com

[3.12.] H. P. Lio and M. S. Yong. New digital phase meter concept and its application. Rev. Sci. Instrum. 1997, 68(4): 1894:1901

[3.13.] Peter L. M. Heydemann. Determination and correction of quadrature fringe measurement errors in interferometers. APPLIED OPTICS. 1981, 20(19):3382-3384

[3.14.] Chien-ming Wu, Ching-shen Su and Gwo-Sheng Peng. Correction of nonlinearity in one-frequency optical interferometry. Meas. Sci. Technol. 1996, 7: 520-524

[3.15.] Christopher Palmer. DIFFRACTION GRATING HANDBOOK (fifth edition). THERMO RGL Richardson Grating Laboratory

[3.16.] JCGM 100: 2008. Evaluation of measurement data- Guide to the expression of uncertainty in measurement. JCGM 2008

[3.17.] Frank C. Demarest. DATA AGE ADJUSTMENTS. United States Patent, 2003, Patent No.: US 6597459B2

[3.18.] Marek Dobosz. High-resolution laser linear encoder with numerical error compensation. Opt. Eng. 1999, 38(6), 968-973

[3.19.] Chyan-Chyi Wu, Wen-Jong Wu, Zheng-Seng Pan, and Chih-Kung Lee. Laser linear encoder with both high fabrication and head-to-scale tolerances. APPLIED OPTICS, 2007 46 (16), 3169-3176

[3.20.] D Shin and B Kim. A laser interferometer encoder with two micromachined gratings generating phase-shifted quadrature.

JOURNAL OF MICROMECHANICS AND MICROENGINEERING. 2011, 21: 085036

[3.21.] Fang Cheng and Kuang-Chao Fan. Linear diffraction grating interferometer with high alignment tolerance and high accuracy. APPLIED OPTICS, 2011, 50 (22): 4550-4556

[3.22.] Ulrich Benner. POSITION-MEASURING DEVICE. United States Patent, 2009, Patent No,: US 7473886 B2

[3.23.] Wolfgang Holzapfel, Andreas Schreiber. POSITION MEASURING DEVICE. United States Patent, 2006, Patent No,: US 7019842 B2

[3.24.] Wofgang Holzapfel, Michael Hermann, Walter Huber, Volker Höfer, Ulrich Benner, Karsten Sändig. INTERFERENTIAL POSITION MEASURING ARRANGEMENT. United States Patent, 2006, Patent No,: US 7154609 B2

[3.25.] Markus Meissner, Joerg Drescher. POSITION-MEASURING DEVICE AND METHOD FOR OPERATING A POSITION-MEASURING DEVICE. United States Patent, 2008, Patent No,: US 7389595 B2

[3.26.] Wolfgang Holzapfel, Udo Linnemann. POSITION MEASURING ARRANGEMENT. United States Patent, 2006, Patent No,: US 7046368 B2

[3.27.] Chyan-Chyi Wu, Cheng-Chih Hsu, Ju-Yi Lee, and Cheng-Yang Liu. Optical Heterodyne Laser Encoder for In-plane Nanopositioning. Proc. of SPIE, 2008, 7063: 70631A

[3.28.] Ju-Yi Lee, Hui-Yi Chen, Cheng-Chih Hsu, Chyan-Chyi Wu. Optical heterodyne grating interferometry for displacement measurement with subnanometric resolution. Sensors and Actuators,2007, A 137: 185-191

[3.29.] Chyan-Chyi Wu, Cheng-Chih Hsu, Ju-Yi Lee, Hui-Yu Chen and Ching-Liang Dai. Optical heterodyne laser encoder with sub-nanometer resolution. Meas. Sci. Technol. 2008, 19: 045305

[3.30.] H L Hsieh, J Y Lee, W T Wu, J C Chen, R Deturche and G Lerondel. Quasi-common-optical-path heterodyne grating interferometer for displacement measurement. Meas. Sci. Technol., 2010, 21: 115304

[3.31.] James Prince. COMPACT LITTROW ENCODER. United States Patent. Patent No,: US 7864336B2

[3.32.] Henry A. Hill. DISTANCE MEASURING INTERFEROMETER AND ENCODER METROLOGY SYSTEMS FOR USE IN LITHOGRAPHY TOOLS. United States Patent. Patent No,: US 7812964B2

[3.33.] Leslie L. Deck, Peter J. De Groot, Michael Schroeder. INTERFEROMETRIC ENCODER SYSTEMS. United States Patent, 2012, Patent No,: US 8300233 B2

[3.34.] Leslie L. Deck, Peter J. De Groot, Michael Schroeder. INTERFEROMETRIC ENCODER SYSTEMS. United States Patent, 2011, Patent No,: US 2011/0255096 A1

[3.35.] Frank C. Demarest. CYCLIC ERROR COMPENSATION IN INTERFEROMTRIC ENCODER SYSTEMS. United States Patent. Patent No,: US 2012/0154780 A1

[3.36.] Leslie L. Deck, Peter J. De Groot, Michael Schroeder. INTERFEROMETRIC ENCODER SYSTEMS. United States Patent, 2012, Patent No,: US 2012/0170048 A1

[3.37.] Yim Bun Patrick Kwan. LITHOGRAPHIC APPARATUS, DEVICE MANUFACTURING METHOD AND DEVICE MANUFACTURED THEREBY. United States Patent, 2009, Patent No,: US 7561270 B2

[3.38.] Erik Roelof Loopstra, Leon Martin Levasier, Rene Oesterholt. LITHOGRAPHIC APPARATUS AND METHOD FOR CALIBRATING THE SAME. United States Patent, 2011, Patent No,: US 7880901 B2

[3.39.] Christopher J. Mason. FOLDED OPTICAL ENCODER AND APPLICATIONS FOR SAME. United States Patent, 2010, Patent No,: US 2010/0290017 A1

[3.40.] Engelbertus Antonius Fransiscus VAN DER PASH, Emiel Jozef Melanic Eussen, Erik Roelof Loopstra. LITHOGRAPHIC APPARATUS AND DEVICE MANUFACTURING METHOD. United States Patent, 2011, Patent No,: US 2011/0116066 A1

[3.41.] Peter Paul Steijaert, Wilhelmus Josephus Box, Emiel Jozef Eussen, Erik Roelof Loopstra, Engelbertus Antonius Van Der Pasch, Ruund Antonius Beerens, Albertus Adrianus Smits.

LIGHTOGRAPHIC APPARATUS HAVING ENCODER TYPE POSITION SENSOR SYSTEM. United States Patent. Patent No,: US 2009/0002653 A1

[3.42.] Marcel Hendrikus Maria Beems, Joe Sakai. LITHOGRAPHIC APPARATUS AND POSITIONING APPARATUS. United States Patent, 2008, Patent No,: US 7349069 B2

[3.43.] Jun Guan, Paul Köchert, Christoph Weichert, Rainer Tutsch. STUDY ON A 1D HOMODYNE ENCODER AND A NOVEL 2D HOMODYNE ENCODER. Proceedings of the 2012 Annual Meeting of the American Society for Precision Engineering (ASPE). 2012, 54: 268-271

[3.44.] Akihide Kimura, Wei Gao and Zeng Lijiang. Position and out-of-straightness measurement of a precision linear air-bearing stage by using a two-degree-of-freedom linear encoder. Meas. Sci. Technol. 2010, 21: 054005

[3.45.] W. Gao, A. Kimura. A fast evaluation method for pitch deviation and out-of-flatness of a planar scale grating. CIRP Annals-Manufacturing Technology. 2010, 59: 505-508

[3.46.] Wolfgang Holzapfel. POSITION-MEASURING DEVICE. United States Patent, 2009, Patent No,: US 7573581 B2

4. A three-channel homodyne interferometric encoder

This encoder is designed to have three measurement channels. All these three channels measure the same displacement (in X-direction) on the same position of the grating scale, through different diffraction orders. It seems that there are some unnecessary redundancies in the design of this encoder, but actually I have the following two reasons for this:

First, the Imperfections and Contaminations of the Grating Scale (ICGS) is one of the contributing factors to the measurement uncertainty of an interferometric encoder. Preliminary simulations indicate that different diffraction orders have different sensitivities to ICGS. All those three channels of this encoder measure exactly the same position on the grating scale, but they employ different diffraction orders of the probing laser beam. The middle channel only uses the first diffraction orders; the other two channels use the

second and zero orders diffracted by the grating scale. To this end, this three-channel encoder provides an opportunity to investigate the suspected different measurement uncertainties of the three channels, which result from the correlations between ICGS and the different diffraction orders. Ultimately, these investigations may offer a possibility to reduce the interferometric encoder measurement uncertainty caused by ICGS. But up to now, this part of investigation has not been carried out.

Second, in the future, this three-channel encoder could be upgraded into a two-dimensional (X and Rz) encoder with minor modification.

4.1. Design code

- **Robust signal:** During the angle measurement (for its 2D version in the future), in the whole angle measurement range (supposed ±10 mrad in Rz), the interference contrast should maintain at a certain level. This will also guarantee that the current 1D three-channel encoder has strong immunity to the angular deviations between the grating scale and the encoder head, in a certain angular deviation range.
- **Easy setup:** For the superposition of the interfering beams, when a channel is aligned, the other two channels should be accordingly automatically aligned.

4.2. Design

4.2.1. Principle and optical design

The schematic of this three-channel homodyne interferometric encoder (simplified as 'TCHOI encoder', the same hereinafter) is shown in Figure 4-1. The TCHOI encoder consists of four modules: light source assembly (LSA), encoder head, grating scale and data processing electronics and application software (DPEAS).

LSA: To reduce the thermal influence of LSA on the performance of the encoder, the LSA is placed distantly away from the encoder head. The laser beam is transmitted through a polarization-maintaining (PM) fiber. In LSA, the laser is a frequency stabilized 532nm laser from INNOLIGHT (product line PROMETHEUS). During this thesis work, only its internal frequency-stabilization function was enabled, which meant a frequency stability of $3.5*10^{-9}$. The half wave plate (1/2λ) and the polarization beam splitter (PBS) are used to adjust the input power of the encoder. The fiber coupler and the PM fiber are from Schäfter+Kirchhoff GmbH.

Encoder head: In the encoder head, the two head gratings (Head Grating L and Head Grating R) and the grating scale are in Littrow configuration, which means that the period of the grating scale is twice of those of the two head gratings which have the same grating parameters including the grating period. After passing a polarizer, the collimated laser beam is directed perpendicularly to the grating scale in the plane XOZ with an out-of-plane angle of α (α =1.6° in this work) to avoid the influence of the zero diffraction order and the unwanted

multi-reflections between head gratings and grating scale, as shown in Figure 4-2.

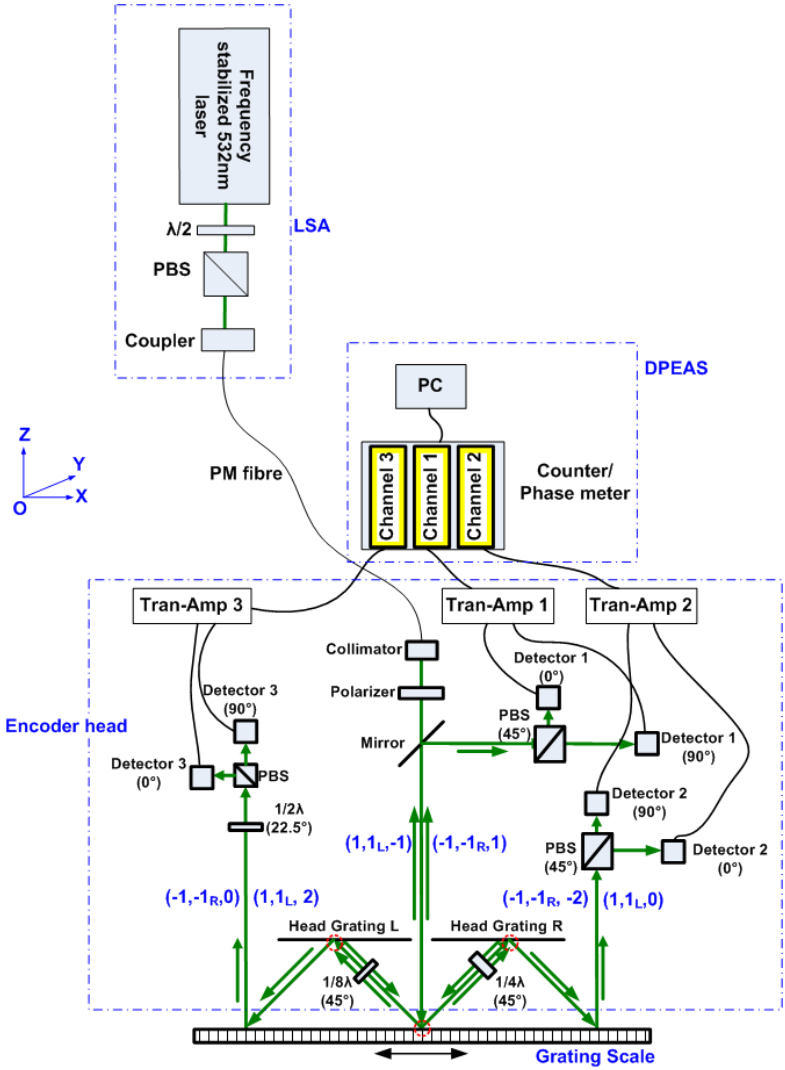

Figure 4-1. Schematic of the three-channel homodyne interferometric encoder; LSA is light source assembly, 1/2λ is half wave plate, PBS is

polarization beam splitter, DPEAS is data processing electronics and application software, PM fiber is polarization-maintaining fiber, PC is personal computer, Tran-Amp is transimpedance amplifier, 1/4λ is quarter wave plate, 1/8λ is octadic wave plate.

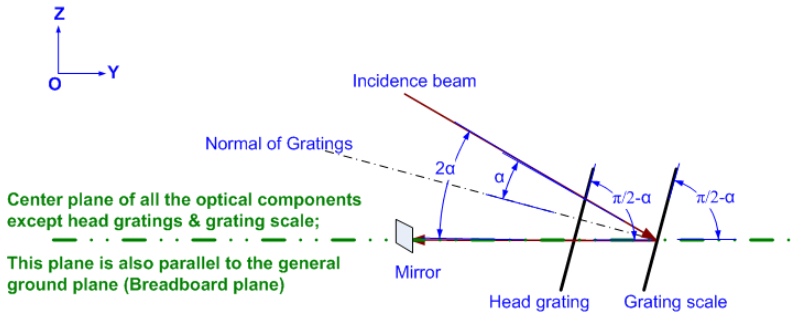

Figure 4-2. Schematic of the out-of-plane incidence angle.

In this TCHOI encoder, only the diffractions, which take place at the three areas marked by red circles in Figure 4-1, are required by its measurement principle. The diffractions, which take place at two unmarked areas in Figure 4-1, are employed only due to geometrical consideration about the encoder head. In the following, only the diffractions required by the measurement principle will be discussed. The diffraction process is a little bit complicated. If this process is still described in traditional pure narrative text, it will be more difficult to be comprehended. As an example, the channel1 is described in pure narrative text: "Following the diffraction on the grating scale, a part of the +1st diffraction order beam is diffracted back to the grating scale again by head grating L along the same path and passes an octadic wave plate (1/8 λ) twice. This 1/8 λ wave plate, the following quarter wave plate (1/4 λ) and PBS are all placed in 45° with respect to the polarization direction of the incoming beam. Similarly, a part of the -

1st diffraction order beam is diffracted back by the head grating R with two passages through a quarter wave plate. Then both beams are diffracted by the grating scale again, and the secondary -1st diffraction order of the former +1st diffraction order beam and the secondary +1st diffraction order of the former -1st diffraction order beam are overlapped and interfere."

Instead of traditional pure narrative text, to better explain the diffraction process, a 3-tuple (or triplet) is employed to represent a diffracted beam. In the 3-tuple: the first element represents the diffraction-order number of the first diffraction on the grating scale, the second element represents the diffraction-order number of the diffraction on the two head gratings, the third element represents diffraction-order number of the second diffraction on the grating scale. Such as, (1, 1_L, 2) represents the beam which goes through following diffraction along the direction of light propagation: the $+1^{st}$ diffraction order after the incidence beam being diffracted by the grating scale for the first time, the $+1^{st}$ diffraction order on the head grating L, the $+2^{nd}$ diffraction order of the diffraction on the grating scale for the second time; (-1, -1_R, 0) represents the beam which goes through following diffraction along the direction of light propagation: the -1^{st} diffraction order after the incidence beam being diffracted by the grating scale for the first time, the -1^{st} diffraction order on the head grating R, the 0 diffraction order (mirror reflection) of the diffraction on the grating scale for the second time.

For channel1 (the middle channel in Figure 4-1), beam (1, 1_L, -1) and beam (-1, -1_R, 1) are overlapped and interfere; the phase information of this interference is corresponding to the relative X-direction

displacement between the grating scale and the encoder head, after detection and phase evaluation the measured displacement can be determined by:

$$D_1 = P*\Phi_1/ (8\pi) \quad (4.1)$$

Where D_1 is the relative displacement detected by channel1; P is the period of the grating scale; Φ_1 is the evaluated phase of the interference of channel1.

Channel2: the interfering beams are beam (-1, -1_R, -2) and beam (1, 1_L, 0). The relative displacement is:

$$D_2 = P*\Phi_2/ (8\pi) \quad (4.2)$$

Where D_2 is the relative displacement detected by channel2; Φ_2 is the evaluated phase of the interference of channel2.

Channel3: the interfering beams are beam (-1, -1_R, 0) and beam (1, 1_L, 2). The relative displacement is:

$$D_3 = P*\Phi_3/ (8\pi) \quad (4.3)$$

Where D_3 is the relative displacement detected by channel3; Φ_3 is the evaluated phase of the interference of channel3.

Theoretically D1, D2 and D3 should be always the same; but in reality they are slightly different due to the different erroneous information of the three different channels. This TCHOI encoder employs quadrature detection technique, for the background knowledge of this technique please refer to the section 2.4. The generation of the related quadrature signals are elaborated in

Appendix A, which are calculated based on the Jones calculus [4.1-4.5].

According to the principle of this TCHOI encoder, beam (1, 1_L, -1), beam (1, 1_L, 0) and beam (1, 1_L, 2) go through the same diffraction process, the only difference among them is that they are the different diffraction orders of the second-diffraction on grating scale; beam (-1, -1_R, 1), beam (-1, -1_R, -2) and beam (-1, -1_R, 0) also go through the same diffraction process, similarly, the only difference among them is also that they are the different diffraction orders of the second-diffraction on grating scale. Beam (1, 1_L, -1) and beam (-1, -1_R, 1) are the interfering beams of channel1; beam (1, 1_L, 0) and beam (-1, -1_R, -2) are the interfering beams of channel2; beam (1, 1_L, 2) and beam (-1, -1_R, 0) are the interfering beams of channel3. Therefore, when interfering beams of channel1 are aligned, channel2 and channel3 will be accordingly automatically aligned, which can be confirmed from the simulation in Lighttools and also has been proven in the experiment of this work. The simulation of this TCHOI encoder in Lighttools is shown in Figure 4-3 as one example. For homodyne encoder the superposition of the interfering beams is critical, since the bad superposition will directly degrade the signal-to-noise ratio. In the sense of superposition of interfering beams, this TCHOI encoder doesn’t require more alignment effort than its single channel version, thanks to the alignment-friendly design of this TCHOI encoder.

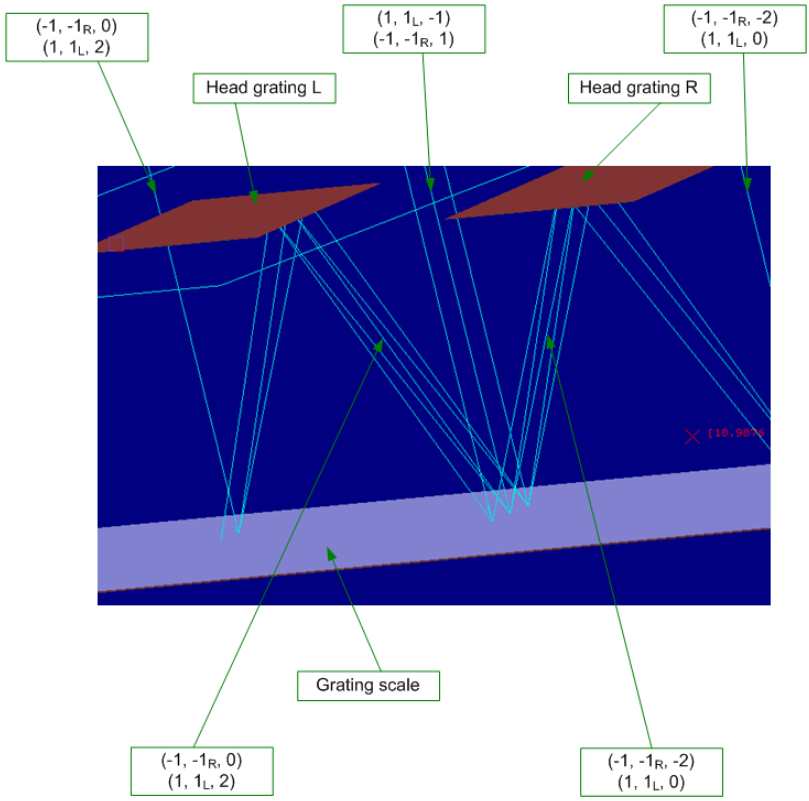

Figure 4-3. Simulation of the TCHOI encoder in Lighttools.

4.2.2. Abbe-error-free line

The Abbe Principle is called the first principle in metrology by some scholars [4.6]. The Abbe Principle was first described by Ernst Abbe of Zeiss and states [4.7]:

If errors of parallax are to be avoided, the measuring system must be placed co-axially (in line with) the line in which displacement (giving length) is to be measured on the work-piece.

Abbe error occurs when the measuring point of interest is displaced laterally from the actual measuring scale location (reference line), and when angular errors exist in the positioning system. Abbe error causes the measured displacement to appear longer or shorter than the true position, depending on the angular offset. The spatial separation between the measured point and reference line is known as the Abbe offset. To ensure zero Abbe error, (for interferometer) the reflector axis of movement should be co-linear with the measurement axis of interest [4.7].

As mentioned in section 3.5, compared to the displacement interferometers, it is more difficult for the interferometric encoders to meet the Abbe principle due to the physical thickness of its grating scale. To overcome this problem, one of my supervisors Dr. Flügge has been looking for encoders which have Abbe-error-free lines behind their grating scales; in this way, when the measurement axes of interest are co-linear with the Abbe-error-free lines, there will be no Abbe errors any more. To work toward this direction, first I try to find a method to identify the Abbe-error-free line of an encoder. For the definition of the Abbe-error-free line in detail, please refer to Appendix B. I used strict manual ray tracing and numerical simulation shown in Appendix B to identify the Abbe-error-free line of an encoder. The Abbe-error-free line of this TCHOI encoder was identified to be its scale axis.

4.2.3. Mechanics

All the elements within the encoder head except the transimpedance amplifiers (Tran-Amp) are fixed on a base plate as shown in Figure 4-4. The base plate and the grating scale holder are fixed on

the optical table which situates in an enclosure during the experiment.

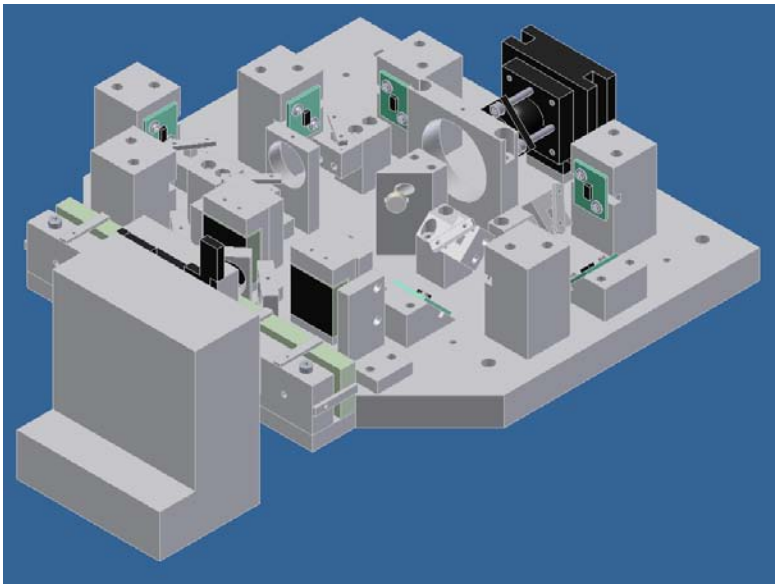

Figure 4-4. Mechanics modeling of the TCHOI encoder head and the grating scale holder in Autodesk inventor.

4.2.4. Electronics and data processing

Tran-Amp: Those Tran-Amps shown in Figure 4-1 are specially designed for quadrature detection applications. They are employed to convert the current signals output from detectors to voltage signals which serve as inputs signals of DPEAS. Each of those original Tran-Amps has four inputs (0°, 180°, 90° and 270°) and two outputs (0° and 90°) through differential amplification. The amplitude-ratio as well as the relative phase between the output 0° and the output 90° is tunable in certain ranges.

To adapt the HEIDENHAIN EIB741 to this TCHOI encoder, a function unit is added to each original Tran-Amp. This function unit splits an input signal into two sub-signals and shifts the phase of one sub-signal by 180°as shown in Figure 4-5.

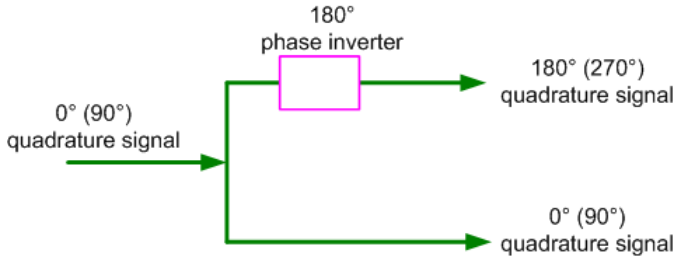

Figure 4-5. Schematic of signal splitting and 180° phase inversion.

DPEAS: During the experiment, two kinds of DPEAS' were investigated: one was HEIDENHAIN EIB741 [4.8] another one was a home-developed phase meter based on fast ADCs [4.9]. The latter one employs 16-bit flash ADCs with signal-to-noise ratio of 80 dB and sampling rate of up to 100 MHz, which result in at least a higher resolution and higher sampling rate compared to EIB741. But the HEIDENHAIN EIB741 has an on-line position correction function which is not implemented in the home-developed phase meter yet up to now.

The application program of EIB741 was programmed in Labview by me. The FPGA program and the application program of the home-developed phase meter were developed by my colleagues.

4.3. Experiment

4.3.1. Comparison measurement with a heterodyne interferometer

To investigate the performance of this TCHOI encoder, a comparison measurement with a differential heterodyne interferometer [4.10] was performed. The comparison measurement setup is shown in Figure 4-6. The grating scale together with the interferometer measurement mirror was fixed on a custom PI (Physik Instrumente) 6-axis piezo stage; the interferometer reference mirror was fixed at the encoder head. In X-direction, this piezo stage has following specifications: 1 nm resolution, 0.03% closed loop linearity (with its built-in capacitance sensors) and 100 µm closed loop travel. During the measurement the piezo stage was continuously moving in X-direction back and forth in a triangle waveform with respect to time. This movement was measured by the TCHOI encoder and the interferometer simultaneously, which were synchronized by a continuous external trigger generated by a function generator. The period of grating scale is 833.3 nm (1200 grooves/mm) and the wavelength of laser is 532 nm. The nominal signal periods of this encoder and the interferometer are 208.3 nm and 266 nm respectively.

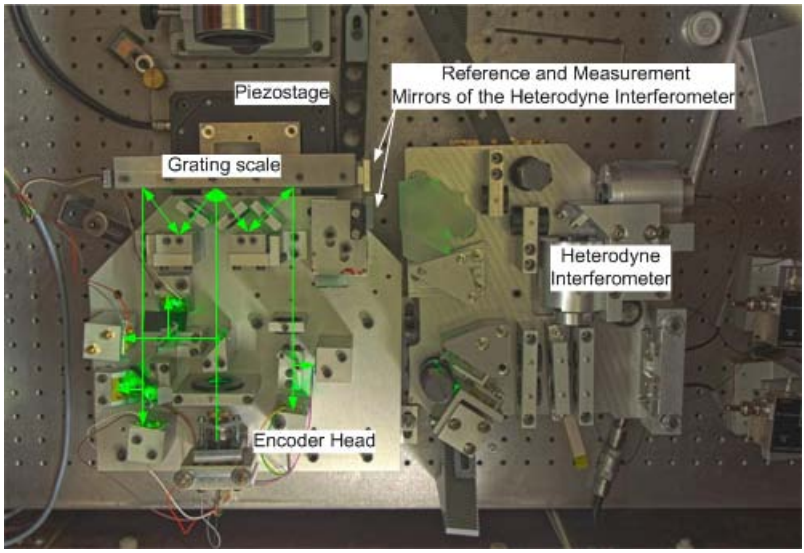

Figure 4-6. The setup for comparison measurement with a differential heterodyne interferometer.

4.3.1.1. EIB741 as DPEAS

When EIB741 was employed, the built-in compensation-for-position-value function [4.8] was enabled. In this comparison measurement experiment, all the periodic nonlinearity results were determined through a fast Fourier transform of the measurement difference between the encoder and the interferometer.

The comparison measurement settings were:

- Encoder/interferometer synchronized at a trigger rate of 10 KHz;
- Piezo stage moving in triangle waveform with amplitude of 5 µm at 0.08 Hz;

- Measurement time: 100 s.

4.3.1.1.1. Channel1

Figure 4-7 (a) shows the measurement difference between the interferometer and channel1 of the TCHOI encoder with a standard deviation of 117 pm. The measurement difference mainly results from the synchronization error, unequal data ages [4.11] between the encoder and the interferometer, periodic nonlinearities of the two measurement systems, signal noise, inhomogeneous fluctuation of refraction index of local ambient air and the different responses of two systems to the motion errors of the piezo stage as well as to the remaining vibration of the optical table. Among them, synchronization error and data-age difference affect the comparison measurement result in the same way. Supposed that the synchronization error and data-age difference are $\Delta\tau s$ and $\Delta\tau da$ respectively, the resulting comparison measurement difference $\Delta msda$ can be expressed by following equation:

$$\Delta msda = v(\Delta\tau s + \Delta\tau da) \qquad (4.4)$$

Here, v is the moving speed of the piezo stage. $\Delta msda$ can basically be identified in the following three ways:

The first two ways are to directly single out $\Delta msda$ from the comparison measurement result. The prerequisite is that the piezo stage should move in triangle waveform with respect to time with a constant repeating frequency during a comparison measurement. Obviously, among all the contributors to comparison measurement difference, only $\Delta msda$ linearly relates to the moving speed of piezo

stage and has the repeating frequency which the piezo stage moves in. Therefore, the waveform of Δmsda should be nearly rectangular like the red data traces in Figure 4-7 (a) and Figure 4-11 (a), since the moving speed of piezo stage was nearly a constant during this experiment. Practically, there are two following ways to directly single out the value of Δmsda from the comparison measurement results: One is to filter the comparison measurement result with a moving average window. When the length of the moving window is selected properly, a rectangular waveform, with the same repeating frequency as the piezo stage moves in, should be obtained. The amplitude of the obtained nearly rectangular waveform is the value of Δmsda. But a more accurate method is to calculate Δmsda directly from the Fourier transformation of the comparison measurement difference without any filtering, which is adopted in this work to determine the value of Δmsda. Δmsda is a nearly rectangular signal with known frequency, which can be easily identified in the amplitude spectrum of comparison measurement difference, which is shown in Figure 4-11 (b) as an example.

The third way is to vary v. When v is varied, the overall comparison measurement difference will vary correspondingly. If v is only varied in a relatively small range, apparently the corresponding variation of the comparison measurement difference is equal to the value Δmsda, since all the aforementioned contributors to comparison measurement difference other than synchronization error and data-age difference will not correlate with the variation of v. Then $\Delta\tau_S+\Delta\tau_{da}$ and Δmsda can be determined.

In this comparison measurement, the identified value of Δmsda is at the order of ± 40 pm (peak to peak).

Figure 4-7 (b) shows the amplitude spectrum of the measurement difference, from which a ± 50 pm overall periodic nonlinearity of the channel1 of this encoder is identified.

According to the nominal moving speed of the piezo stage and the nominal signal periods of the differential heterodyne interferometer and the TCHOI encoder, the nominal first order (fundamental) nonlinearity frequency of the interferometer is 6.01 HZ, the nominal first order nonlinearity frequency of the TCHOI encoder is 7.68 Hz. According to reference [4.10], the periodic nonlinearity of the differential heterodyne interferometer was less than ± 10 pm only at second order frequency: But during this experiment, the periodic nonlinearity of the interferometer turned out to be ± 20 pm at the first order frequency as shown in Figure 4-7 (b); this was because that during this comparison measurement, the interferometer was aligned and adjusted by myself who didn't have as thorough knowledge about this interferometer as the developer Christoph Weichert has. According to the analysis in reference [4.10], the ± 20 pm first order nonlinearity was introduced by the multi-reflection inside the interferometer.

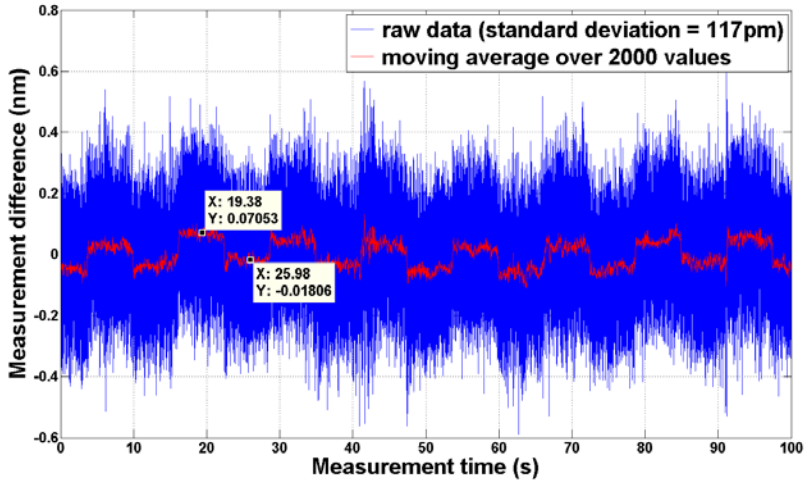

(a)

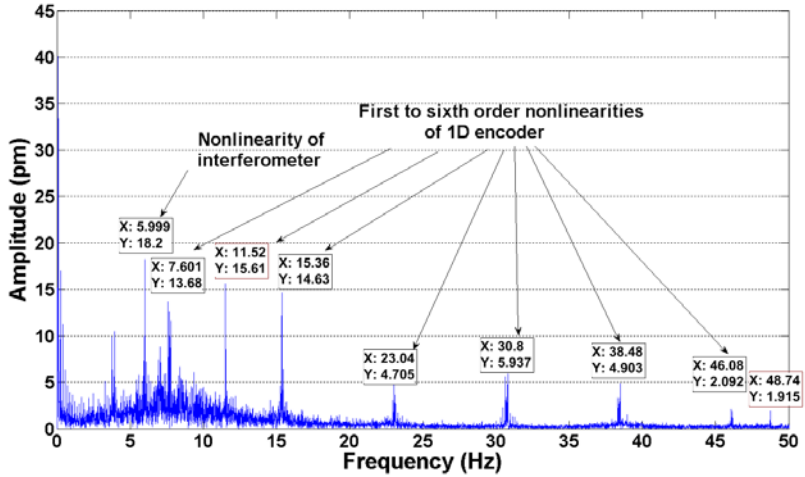

(b)

Figure 4-7. (a) Measurement difference between the interferometer and channel1 of the TCHOI encoder with EIB741; (b) Amplitude spectrum of (a); X: horizontal axis, Y: vertical axis

As shown in Figure 4-7 (b), the periodic nonlinearities of the TCHOI encoder also show up at unusual orders of frequency such as the third to the sixth orders and even 0.5, 1.5 and 6.5 orders. But when the EIB741 was replaced by the home-developed phase meter with off-line Heydemann correction [4.12], there was only first order of periodic nonlinearity, as shown in Figure 4-11 (b) in the following section 4.3.1.2. During this work, the off-line Heydemann correction was performed in the following way: for one file of raw data acquired during the whole comparison measurement time, the correction parameters were calculated only once and applied for all data points. The Heydemann correction only corrects the first and the second order periodic nonlinearities [4.12]. Therefore, apparently the aforementioned unusual orders of periodic nonlinearities are caused by the dynamic position-compensation mechanism of HEIDENHAIN EIB741 [4.8] which dynamically changes the position-compensation parameters during the measurement.

4.3.1.1.2. Channel2

As shown in Figure 4-8, the channel2 has a synthetic periodic nonlinearity of ±150 pm. For channel2, both the measurement difference and the periodic nonlinearities are bigger compared with those of channel1. This is because in channel2 or channel3 the two interfering beams have 60 percent intensity difference which will lower the contrast of the detected signal. To optimize the design of this TCHOI encoder in the future, the disparity of the intensities of the interfering beams can be removed optically; and the influence of this disparity also can be reduced through the optimization of the Tran-Amps.

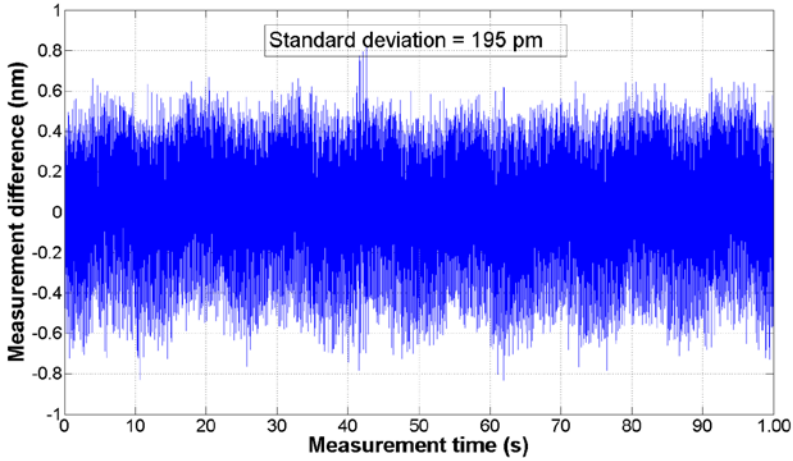

(a)

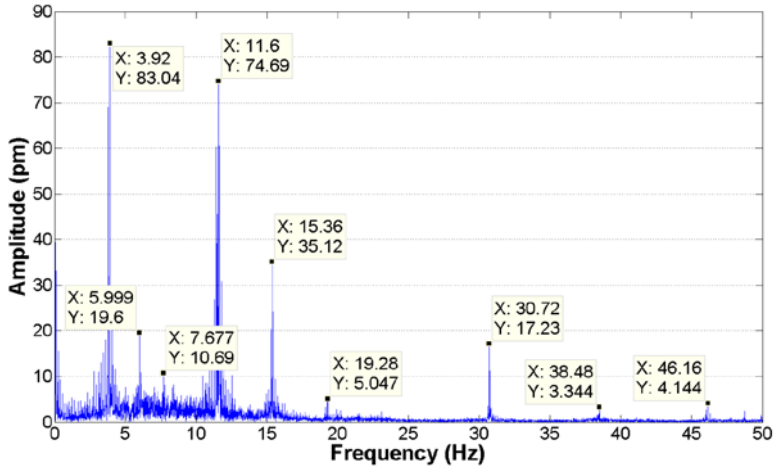

(b)

Figure 4-8. (a) Measurement difference between the interferometer and channel2 of the TCHOI encoder with EIB741; (b) Amplitude spectrum of (a); X: horizontal axis, Y: vertical axis.

4.3.1.1.3. Channel3

As shown in Figure 4-9 (b), channel3 has a synthetic periodic nonlinearity of ±70 pm. The performance of the channel3 is also worse than that of the channel1 but better than that of channel2. The dominating factor, which causes the performance difference between channel2 and channel3, is the unequal performance between Tran-Amp2 and Tran-Amp3; this can be proven by exchanging the Tran-Amp2 and the Tran-Amp3 during the experiment. Theoretically, only the ICGS will cause the different performance between channel1 and channel2/3.

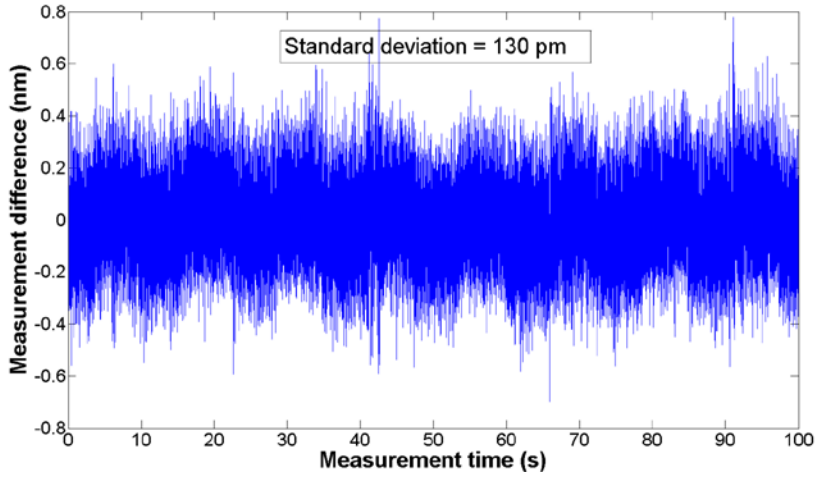

(a)

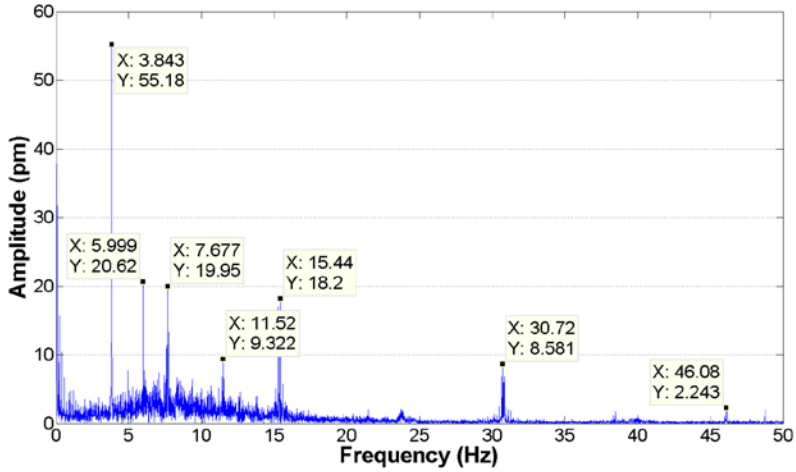

(b)

Figure 4-9. (a) Measurement difference between the interferometer and channel3 of the TCHOI encoder with EIB741; (b) Amplitude spectrum of (a); X: horizontal axis, Y: vertical axis.

4.3.1.1.4. Difference between three channels

In the future, to experimentally investigate the suspected different sensitivities of the three channels to the ICGS, the influence of unequal performance between detectors and electronics of the three channels should be reduced as much as possible. And then that influence can be further reduced by exchanging those detectors and electronics before repeating the comparison measurements. But the prerequisite is that the piezo stage has good enough repeatability.

However, during this experiment, the aforementioned pre-conditions were not met, which can be seen from Figure 4-10. Figure 4-10 (a) shows the amplitude spectra of the measurement difference between

the interferometer and the TCHOI encoder for all the three channels, the absolute differences between those amplitude spectra are displayed in Figure 4-10 (b). From Figure 4-10 (b), we can see that the dominating factors for the difference between channels are electrical factors which have very sharp peaks in the amplitude spectrum differences.

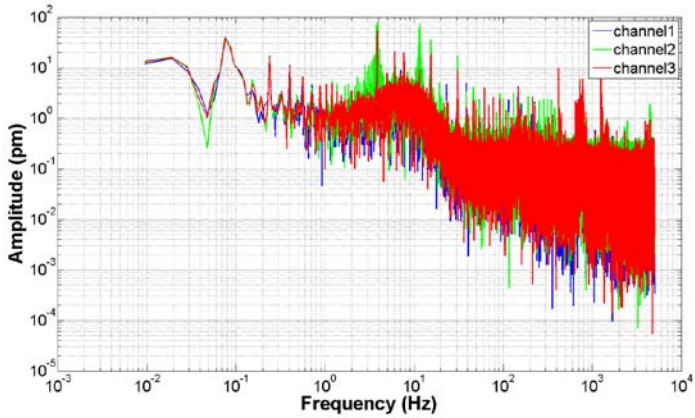

(a)

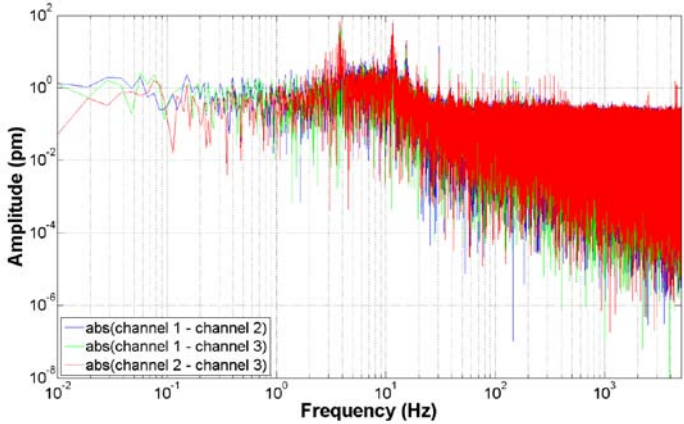

(b)

Figure 4-10. (a) Amplitude spectra of the measurement difference between the interferometer and the three channels of the TCHOI encoder; (b) absolute differences between amplitude spectra shown in (a).

4.3.1.2. Home-developed phase meter as DPEAS

When the home-developed phase meter was used as DPEAS of this encoder, an off-line Heydemann correction was also performed: for one file of raw data acquired during the whole comparison measurement time, the correction parameters were calculated only once and applied to all data points.

The following measurement settings were used:

- Encoder and interferometer employ the same phase meter with data acquisition rate of 48,828 kHz;
- The piezo stage was moving in a triangle waveform with amplitudes of 5 µm at 0.1 Hz ;
- Measurement time: 122.4 s.
- Only channel1 is employed due to the limited adapted connectors from the Tran-Amp to the home-developed phase meter.

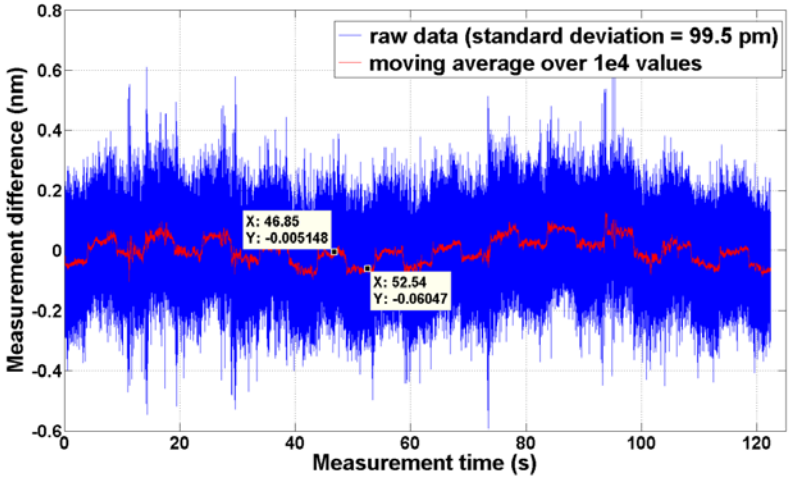

(a)

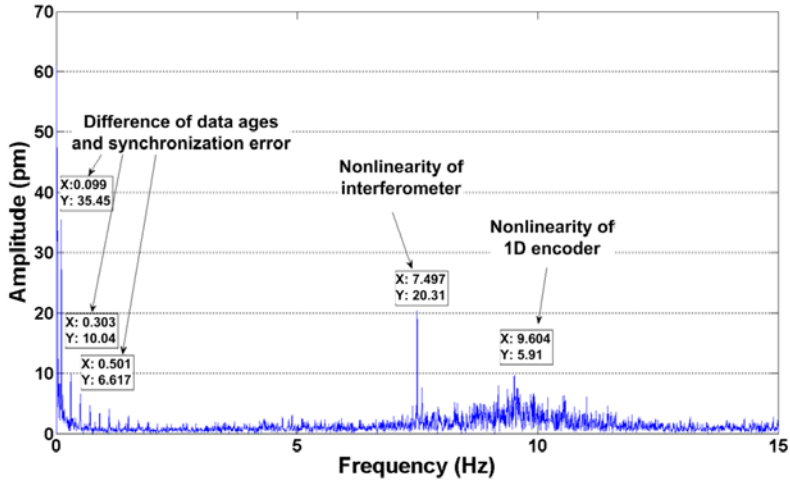

(b)

Figure 4-11. (a) Measurement difference between the interferometer and channel1 of the TCHOI encoder with the phase meter; (b) Amplitude spectrum of (a); X: horizontal axis, Y: vertical axis.

The standard deviation of the measurement difference between the interferometer and channel1 of the TCHOI encoder is 100 pm, as shown in Figure 4-11 (a). During this experiment, the interferometer and channel1 of the TCHOI encoder used the same phase meter, which should result in a lower synchronization error between these two systems than before. But the interferometer and the TCHOI encoder still employed different optical layouts, detectors and pre-amplifiers, which contribute to the data-age difference. The value of Δmsda in the order of ± 30 pm (peak to peak) was still identified. However compared to the result of last comparison measurement, the value of Δmsda is only improved by the order of ±10 pm (peak to peak), which was not as significantly as we expected. Later on we found out that this was due to our program slip in the FPGA program. But unfortunately when the program slip was found and solved, the TCHOI encoder was already dismantled and some its parts were used in a heterodyne encoder experiment which will be described in the following chapter 6. The amplitude spectrum of the measurement difference shows that the overall periodic nonlinearity of this encoder now is less than ± 10 pm (with aforedescribed off-line Heydemann correction), which is shown in Figure 4-11 (b).

4.3.2. System stability

4.3.2.1. Short term (3 minutes)

Unfortunately, before this TCHOI encoder was dismantled, only the short term system stability of its channel2 was measured. The measurement settings were:

- The TCHOI encoder situated in the upstairs laser source room of our laboratory;
- The grating scale was fixed on the piezo stage which was in open loop.
- Measurement time: 180 seconds.

Under this condition, the three-minute system stability of the channel2 of this TCHOI encoder is 0.139 nm of standard deviation, as shown in Figure 4-12. But due to the non-optimized measurement condition, this measurement result only provided a general comprehension about the system stability of this TCHOI encoder. Therefore, it is not necessary to further analyze this system stability measurement result. As for the heterodyne interferometric encoder, which will be presented in chapter 6, the system stability measurement condition is optimized and the analysis about its system stability measurement result also will be provided.

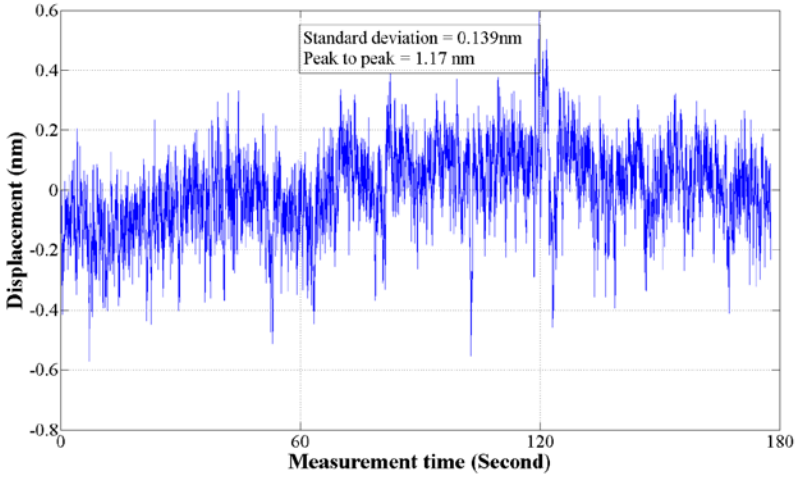

Figure 4-12. Three-minute system stability of the channel2 of the TCHOI encoder.

4.3.2.2. Long term (35 hours)

The long term (35 hours) system stability of the TCHOI encoder was performed with following settings:

- Only the measurement of channel1 was recorded (concerning the total size of the recorded data);
- The comparison measurement setup was used, in which the piezo stage was in open loop;
- The setup was situated in a enclosure;
- Measurement time: 35 hours.

The result is shown in Figure 4-13. The main reason for those drifts was the temperature rising caused by the heat dissipation of the pre-amplifiers and detectors inside the enclosure. As shown in Figure 4-13, the stability of the TCHOI encoder was clearly better than that of the differential heterodyne interferometer. But both the TCHOI encoder and the interferometer were far from end products, especially their mechanical parts which would result in system drifts under temperature deviations.

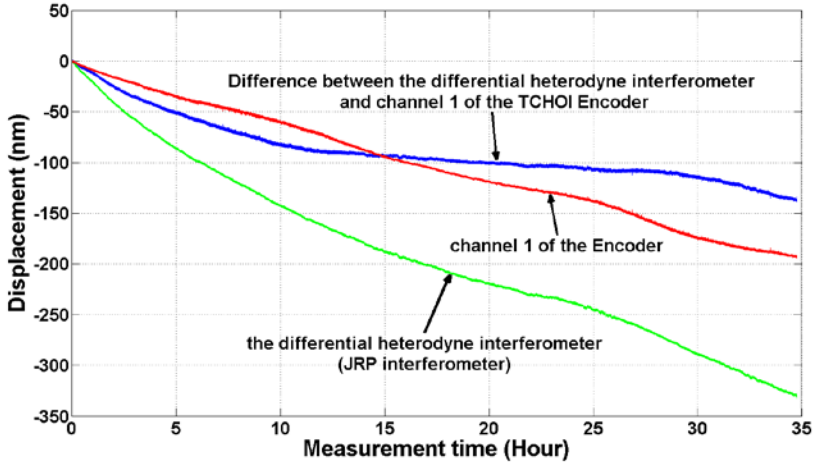

Figure 4-13. Long term (35 hours) system stability of the channel1 of the TCHOI encoder.

4.4. Conclusion

A TCHOI homodyne encoder was developed and investigated. If a home built phase meter based on fast ADCs together with off-line Heydemann correction were employed, its channel1 exhibited a periodic nonlinearity of less than ± 10 pm; in the case a HEIDENHAIN EIB741 was used as its DPEAS, a synthetic periodic nonlinearity of ± 50 pm of its channel1, a synthetic periodic nonlinearity of ± 150 pm of its channel2 and a synthetic periodic nonlinearity of ± 70 pm of its channel3 were observed. The poorer performance of its channel2 and channel3 were due to their lower signal contrast which can be improved optically or electronically in the future.

This TCHOI encoder also can provide an opportunity to investigate the suspected different measurement uncertainties of the three channels, which result from the corresponding correlations between ICGS and the different diffraction orders. But to enable and facilitate this investigation, the TCHOI encoder should be optimized to have equal performance among its three channels in the future.

References

[4.1.] R. CLARK JONES. A New Calculus for the Treatment of Optical Systems I. Description and Discussion of the Calculus. J. O. S. A., 1941, 31: 488-493

[4.2.] R. CLARK JONES. A New Calculus for the Treatment of Optical Systems II. Proof of Three General Equivalence Theorems. J. O. S. A., 1941, 31: 493-499

[4.3.] R. CLARK JONES. A New Calculus for the Treatment of Optical Systems III. The Sohncke Theory of Optical Activity. J. O. S. A., 1941, 31: 500-503

[4.4.] R. CLARK JONES. A New Calculus for the Treatment of Optical Systems V. A More General Formulation and Description of another Calculus. JOURNAL OF THE OPTICAL SOCIETY OF AMERICA, 1947, 37(2): 107-110

[4.5.] R. CLARK JONES. A New Calculus for the Treatment of Optical Systems VII. Properties of the N-Matrices. JOURNAL OF THE OPTICAL SOCIETY OF AMERICA, 1948, 38(8): 671-685

[4.6.] G. X. Zhang. A Study on the Abbe Principle and Abbe Error. Annals of the CIRP, 1989, 38(1): 525-528

[4.7.] Richard Leach. FUNDAMENTAL PRINCIPLES OF ENGINEERING NANOMETROLOGY. ELSEVIER, 2010, ISBN-13: 978-0-08-096454-6

[4.8.] HEIDENHAIN. User's Manual EIB741 External Interface Box for Connecting HEIDENHAIN Encoders. December 2010

[4.9.] P Köchert, J Flügge, Ch Weichert, R Köning and E Manske. Phase measurement of various commercial heterodyne He-Ne-laser interferometers with stability in the picometer regime. Measurement Science and Technology. 2012; 23: 074005

[4.10.] C Weichert, P Köchert, R Köning, J Flügge, B Andreas, U Kuetgens and A Yacoot. A heterodyne interferometer with periodic nonlinearities smaller than ±10pm. Measurement Science and Technology. 2012, 23: 094005

[4.11.] Frank C Demarest. High-resolution, high-speed, low data age uncertainty, heterodyne displacement measuring interferometer electronics. Measurement Science and Technology. 1998, 9: 1024-1030

[4.12.] Peter L.M.Heydemann. Determination and correction of quadrature fringe measurement errors in interferometers. Applied Optics. 1981; 20 (19): 3382-3384

5. A two-dimensional homodyne interferometric encoder

5.1. Design code

- The grating scale is a one-dimensional grating;
- The measurement standard along X-axis is the period of the grating scale;
- At least part of the measurement standard along Z-axis should be the period of the grating scale;
- In principle, there should be no signal-contrast degeneration in the measurement ranges along both axes.

5.2. Design

The principle of the two-dimensional homodyne interferometric encoder is schematically shown in Figure 5-1. The encoder head consists of a beam splitter and two modules which are mirror-symmetric with respect to the normal of the grating scale. The incoming beam is split into two beams which serve as incoming beams for module 1 and module 2 respectively. At module 1, the incidence beam strikes the grating scale with an incidence angle θ, which is chosen to meet the grating equation:

$$P^* \sin(\theta) = \lambda \tag{5.1}$$

In which, P is the period of the grating scale; λ is laser wavelength. After diffraction on the grating scale, the +1st diffraction order beam propagates along the normal of the grating scale; and the 0th order strikes on the reflector and is reflected back to the grating scale again along the same path, which results in a double passage through a wave plate. Then that 0th order is diffracted on the grating scale again. The secondary -1st diffraction order of the former 0th diffraction order beam and the aforementioned +1st diffraction order beam are overlapped and interfere. Module 2 is likewise.

If there are relative displacements Δx in X-and Δz in Z-direction between encoder head and grating scale, following phase changes will be detected:

$$\Delta\Phi 1 = -4\pi^* \Delta x/P + 2\pi(4/\tan(2\theta) + 2\tan(\theta))\, \Delta z/P \tag{5.2}$$

$$\Delta\Phi 2 = -4\pi^* \Delta x/P - 2\pi(4/\tan(2\theta) + 2\tan(\theta))\, \Delta z/P \tag{5.3}$$

ΔΦ1 and ΔΦ2 are the phase changes sensed by Module 1 and Module 2 respectively. Based on equation (5.2) and (5.3), Δx and Δz can be calculated:

$$\Delta x = -P(\Delta\Phi 1 + \Delta\Phi 2)/(8\pi) \quad (5.4)$$

$$\Delta z = P(\Delta\Phi 1 - \Delta\Phi 2)\tan(2\theta)/(4 + 2\tan(2\theta) * \tan(\theta))/(4\pi) \quad (5.5)$$

Therefore, according to equation (5.4) and (5.5), Δx and Δz can be simultaneously measured by this two-dimensional homodyne interferometric encoder. The signal periods are P/2 in X-direction and P*tan(2θ)/(4+2*tan(2θ)*tan(θ)) in Z-direction. The measurement range in Z direction is limited by the size of detectors and the relevant geometrical relationship.

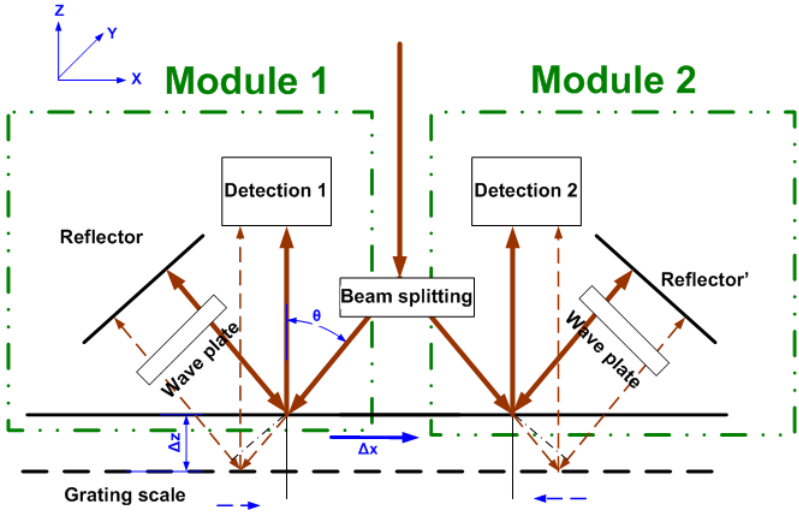

Figure 5-1. Schematic of the two-dimensional homodyne interferometric encoder.

5.3. Proof-of-principle experiment

Due to time limitation, only two days were spent on the experiment of this two-dimensional interferometric homodyne encoder. Up to now only the experiment of one module was performed to prove the principle of this two-dimensional homodyne interferometric encoder. The setup is shown in Figure 5-2. The period of grating scale and the wavelength of laser are the same as those of TCHOI encoder experiment.

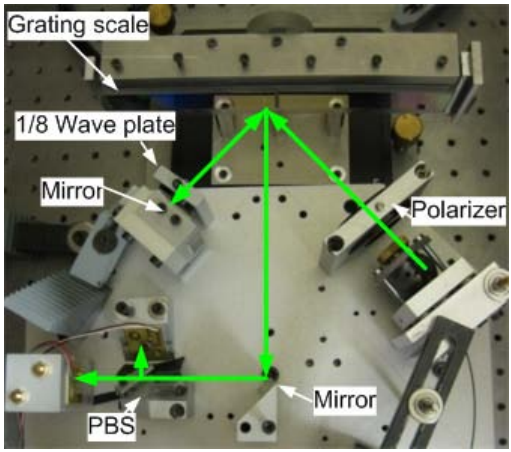

Figure 5-2. Setup of the proof-of-principle experiment of the two-dimensional homodyne interferometric encoder.

During this experiment, the piezo stage continuously moved in triangle waveform with amplitude of 5 μm at a rate of 0.1 Hz in X-or Z-direction. The signal periods of the two-dimensional homodyne interferometric encoder are 416.67 nm in X-direction and 345.59 nm (θ = 39.67°) in Z-direction. The design measurement range in Z direction is ± 1.5 mm.

Since the main purpose of this experiment is only to provide a preliminary proof of its principle, a number of provisional solutions have been adopted. Therefore quite high nonlinearities: ± 80 nm in X-direction and ± 60 nm in Z-direction were identified, as shown in Figure 5-3 which displays the residuals of the linear fit of the encoder readings, supposed the positioning errors of the piezo stage are relatively negligible in this case. Despite those high nonlinearities, the principle of this two-dimensional homodyne interferometric encoder was preliminarily proved.

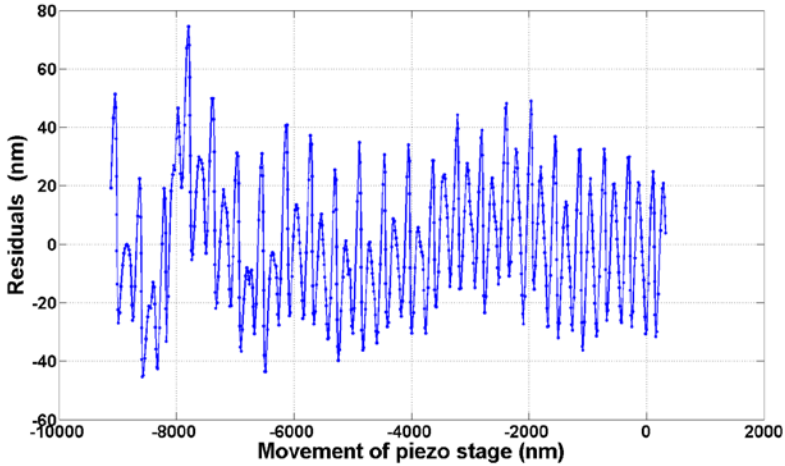

(a)

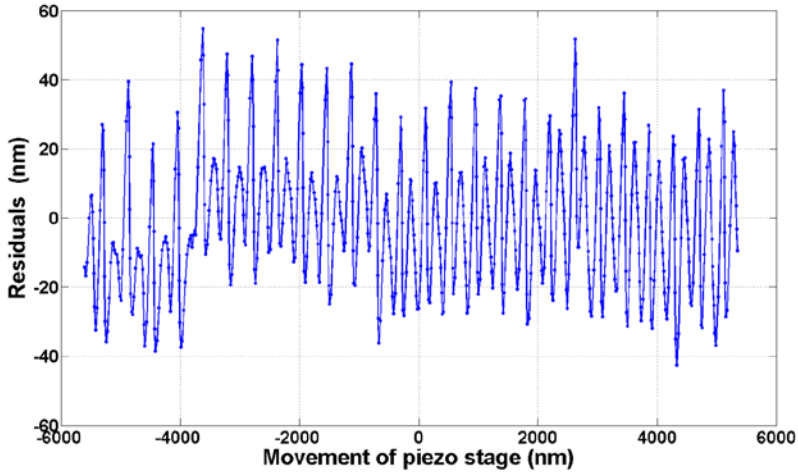

(b)

Figure 5-3. Nonlinearities of the two-dimensional encoder: (a) in X-direction; (b) in Z-direction.

5.4. Conclusion

A novel two-dimensional interferometric homodyne encoder was devised. Along X-axis, its measurement standard was the period of the grating scale; along Z-axis, the measurement standard was the synthesis of the period of the grating scale and the wavelength of the laser. Its proof-of-principle experiment was carried out.

6. A differential heterodyne interferometric encoder

6.1. Design code

- One channel is used to measure the displacement of the grating scale which is attached on the measurand; another channel is used to simultaneously sense the erroneous information introduced by the laser source assembly, environmental fluctuations and the detection unit. To reduce the periodic nonlinearities introduced by the polarization mixing, in each channel, the interfering beams are spatially separated before they superimpose and interfere.

6.2. Design

6.2.1. Principle

The schematic of the differential heterodyne interferometric encoder (simplified as “DIHEI encoder”, the same hereinafter) is shown in Figure 6-1. This DIHEI encoder is composed of four modules: light source assembly (LSA), encoder head, grating scale and data processing electronics and application software (DPEAS). The laser source is a frequency-doubled Nd:YAG laser with output wavelength of 532nm. After successively passing through the first half-wave plate, the first polarizing beam splitter (PBS) and the second half-wave plate, the linear polarized laser light is split into two parts by the second PBS. The first half-wave plate and the first PBS are used to adjust the inputting light intensity of the DIHEI encoder. The frequencies of these two parts of light are shifted by two acousto-optic modulators (AOM1 and AOM2) respectively. During this experiment, AOM1 and AOM2 were driven by a two-channel function generator in 78 MHz and 80 MHz respectively. Then these two parts of frequency-shifted laser light are delivered to the encoder head through two polarization maintaining (PM) fibers, which spatially separates the LSA from the encoder head to reduce the LSA thermal influence on the encoder head. After reaching the encoder head, these two linear polarized beams, which have parallel polarization direction, are directed to a non-polarization beam splitter (NPBS) with the same out-of-plane angle with respect to the plane XOZ. This out-of-plane angle is not shown in Figure 6-1 but can be perceived in following Figure 6-2 (b). When these two incidence light beams are projected on the plane of XOZ, they have mirror symmetry with

respect to the normal of NPBS. After being split by the NPBS, two reflection beams are superposed at a non-polarization beam combiner (BC) and one part of the overlapping and interfering light is detected by detector2. Another two parts of light, which pass through the NPBS, strike the same position on the grating scale which is attached on the measurand. After diffraction on the grating scale, the +1 diffraction order beam of one incidence light beam and the -1 diffraction order beam of another one overlap and interfere, followed by detection by detector1. Detector1 and detector2 are connected with channel1 and channel2 of the phase meter respectively.

Obviously channel2 only detects the erroneous phase information which is introduced by LSA, the ambient environment fluctuations and detection unit. Channel1 senses both the phase information introduced by the relative movement in X-direction between the encoder head and the grating scale as well as the erroneous information introduced by all the contributors listed in the following Table 6-1 (in the following section 6.4). When the gap between the grating scale and the encoder head is small enough, the erroneous phase information sensed by channel1 is close to that sensed by channel2. Therefore, in principal, to quite high content, the differential information between channel1 and channel2 only results from the relative displacement between encoder head and grating scale in X-direction. In this design, the two pairs of interfering beams are spatially separated before they superimpose and interfere, which will reduce the periodic nonlinearities resulting from the polarization mixing. Its simulation in Lighttools is shown in Figure 6-2.

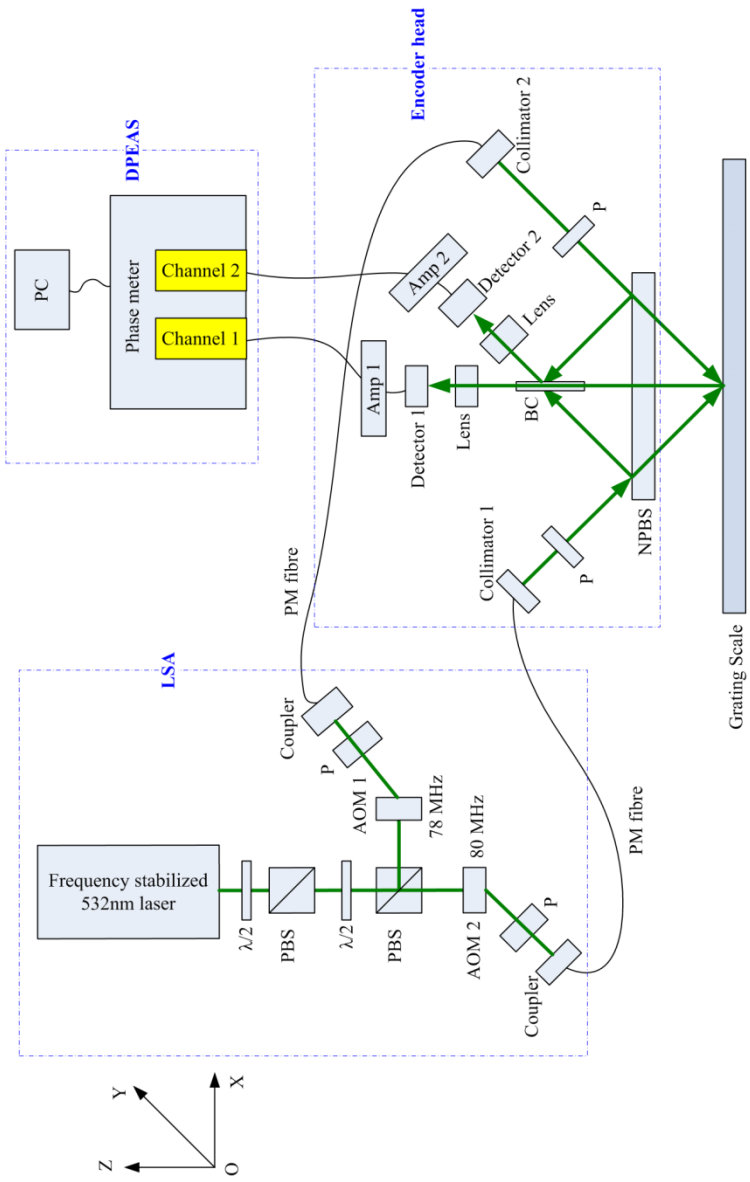

Figure 6-1. Schematic of the DIHEI encoder; λ/2 is half wave-plate, PBS is polarization beam splitter, AOM is acousto-optic modulator, P is polarizer,

NPBS is non-polarization beam splitter, BC is beam combiner, Amp is transimpedance amplifier, PM is polarization maintaining, LSA is light source assembly, DPEAS is data processing electronics and application software.

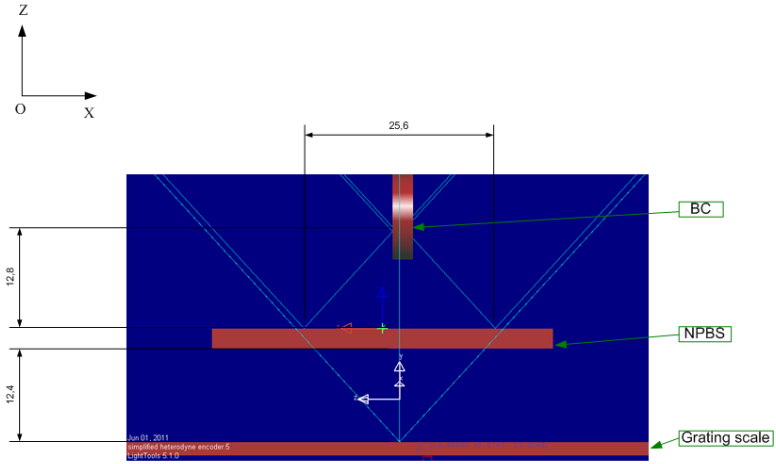

(a)

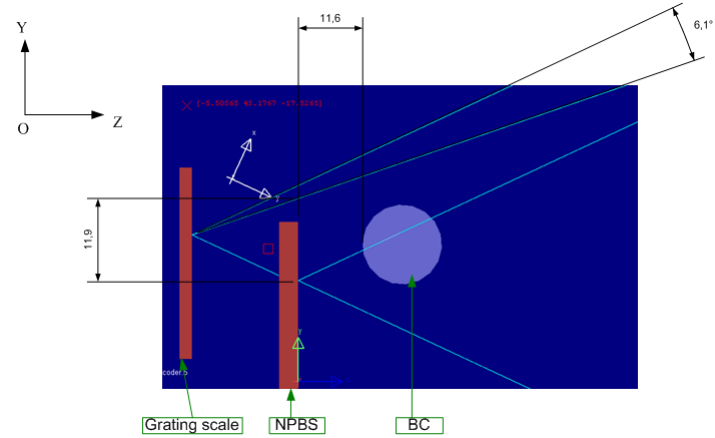

(b)

Figure 6-2. The simulation of the DIHEI encoder in Lighttools; (a) in plane XOZ, (b) in plane YOZ.

In this work, the grating scale was a plane holographic reflectance grating with period of 1200 groves/mm from Richardson Gratings. Two S5971 Si PIN photodiodes from HAMAMATSU were chosen as photo detectors of this DIHEI encoder; and the transimpedance amplifiers were two FEMTO HCA-10M-100K. The phase meter was a home-developed one [6.1]. This phase meter has eight input channels. Each channel is based on a 16-bit flash ADC (analogue-to-digital converter) and each two channels are connected to a FPGA unit. The ADCs have a signal-to-noise ratio of 80 dB and sampling rate of up to 100 MHz. The phase evaluation, which is based on lock-in principle, is implemented in the FPGA units. In this work, the beat frequency of the DIHEI encoder was 2 MHz (80 MHz -78 MHz). A low-pass filtering was embodied by an averaging window with a window length of 1800 values. Therefore, the actual data acquisition rate of this phase meter was 55.556 kHz.

6.2.2. Mechanics

The mechanics design is shown in Figure 6-3, which was modeled in Autodesk Inventor.

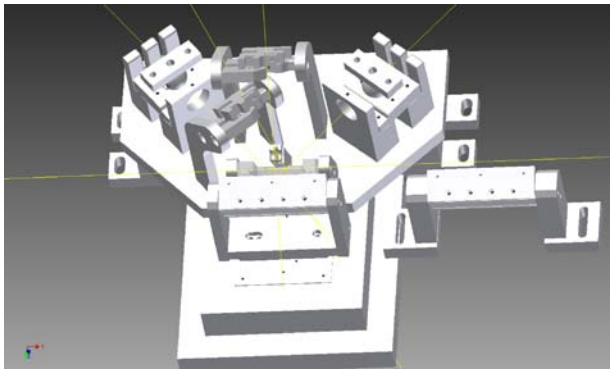

Figure 6-3. Modeling of the DIHEI encoder mechanics in Autodesk Inventor.

6.3. Experiment

6.3.1. System stability

To characterize the performance of this DIHEI encoder, first of all, a 30-second short term and a one-hour long term system stability tests were performed. During the system stability tests, both the DIHEI encoder head and the grating scale were fixed on an optical table which was situated in an enclosure.

Figure 6-4 shows that over 30 seconds the DIHEI encoder has a system stability of 38 pm standard deviation and 289 pm peak-to-peak-value. This 30-seconds system stability more indicates the overall electrical noises levels of the DIHEI encoder, as shown in Figure 6-5. Among all the electrical noises: the noise of the phase meter itself is 31µrad (standard deviation) [6.1], which corresponds to a DIHEI-encoder noise of 2 pm; the shot noise of the DIHEI encoder is 8.6 nm, which is calculated with the method that is used to

evaluate a prior reported heterodyne interferometer [6.2]; the calculated noise, which result from the thermal noise of the detector and the noise of the transimpedance amplifier, is 0.8 pm. But other parts of the DIHEI encoder noises, which are introduced by the electrical noise of the AOM drivers and the electrical noise of the laser device, are not analyzed yet up to now. The concrete causes for the peaks shown in Figure 6-5 are also not clear up to now.

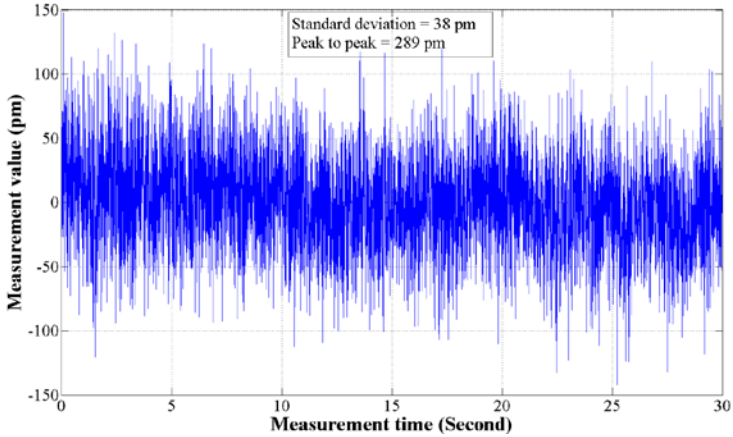

Figure 6-4. The system stability of the DIHEI encoder over 30 seconds.

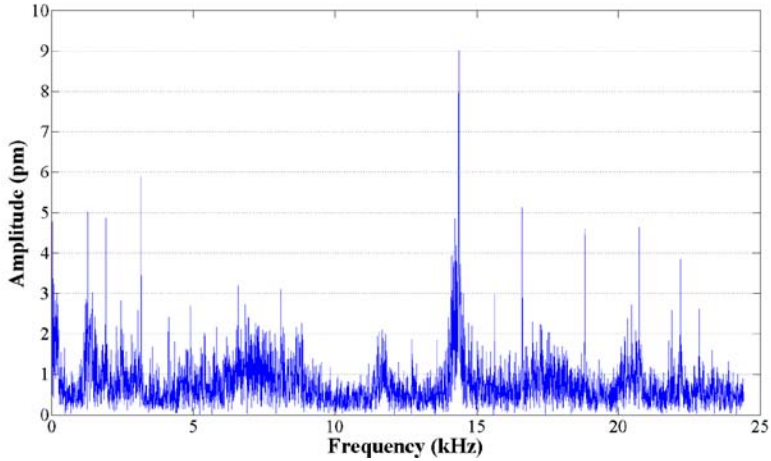

Figure 6-5. The amplitude spectrum of the 30-second system stability shown in Figure 6-4.

Since this DIHEI is designed according to differential principle, it is expected to have a good immunity to the environmental fluctuations and vibrations. For the DIHEI encoder immunity to the environmental fluctuations and the vibrations, it can be demonstrated through the one-hour system stability test. The one-hour system stability was performed after the enclosure was closed for 12 hours. The result of the one-hour system stability test is provided in Figure 6-6, which shows that in one hour the DIHEI encoder has a system stability of 0.1 nm standard deviation and 0.808 nm peak-to-peak value. The amplitude spectrum of this one-hour stability is shown in Figure 6-7.

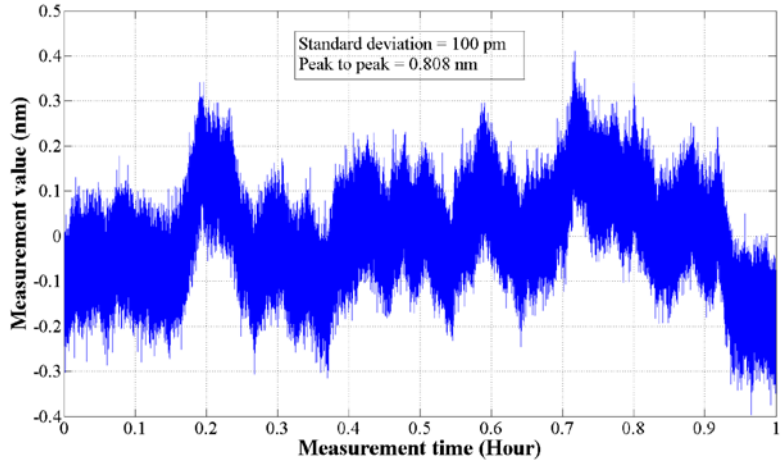

Figure 6-6. The system stability of the DIHEI encoder in one hour.

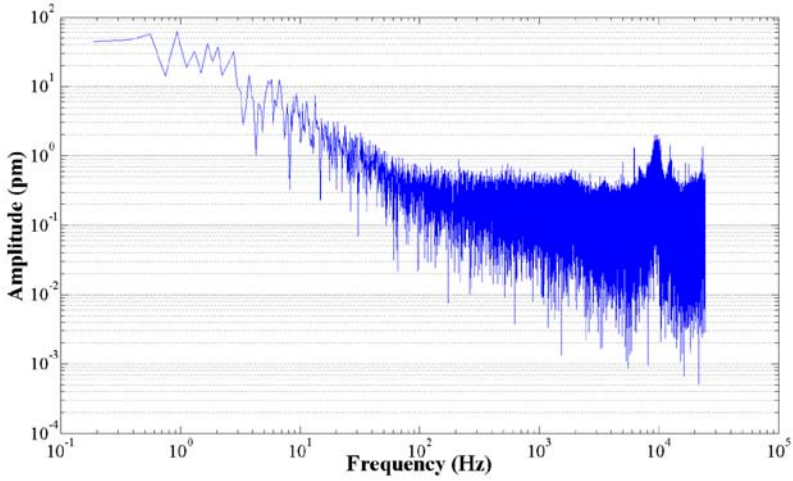

Figure 6-7. The amplitude spectrum of the one-hour system stability shown in Figure 6-6.

6.3.2. Comparison measurement with a heterodyne interferometer

To identify the periodic nonlinearities of this DIHEI encoder, a comparison measurement with a differential heterodyne displacement interferometer was performed. The schematic of the comparison measurement setup is shown in Figure 6-8. The grating scale of the DIHEI encoder and the measurement mirror (MM) of the interferometer are rigidly fixed to each other, and then they are mounted on the piezo stage. The piezo stage is a custom PI (Physik Instrumente) 6-axis piezo stage. In X-direction, this piezo stage has following specifications: 1 nm resolution, 0.03% closed loop linearity (with its built-in capacitance sensors) and 100 µm closed loop travel. The piezo stage controller is a PI E-712.6CDA.

To reduce the synchronization error between the DIHEI encoder and the interferometer and also to enhance the performance of the interferometer, phase values of both the DIHEI encoder and the interferometer were evaluated by the same home-developed phase meter which has eight input channels.

The optics of this interferometer is built based on the Zygo DPMI [6.3] which is a double path differential heterodyne displacement interferometer. The laser source of this interferometer is Zygo AXIOM 2/20 laser source which is a Helium-Neon frequency stabilized laser with two vacuum wavelengths of 632.991501nm and 632.991528 nm. The wavelength of the laser light is the length standard for this interferometer. The laser beam generated by this laser source contains two components with following characteristics: (a) collinear

(both component beams travel on the same path); (b) orthogonally polarized; (c) frequencies differ by 20 megahertz. The frequency stability of this laser source over the lifetime of its laser tube is expected to be better than one part in 10^7 [6.3].

In Figure 6-8, after passing through a half waveplate (HW), the laser light is split into two parts by a non-polarization beam splitter (NPBS). One part is directed into the reference channel which consists of a polarizer (P), focusing lens (FL) and a photoreceiver (PR). Another part is used by the measurement channel which is composed of Zygo DPMI optics, reference mirror (RM), measurement mirror (MM), fold mirror, polarizer, focusing lens and photoreceiver, successively in the direction of light propagation. In our setup, the two photoreceivers were PR130 photoreceivers from GIGAOPTICS. The photography of the opto-mechanical parts of the comparison setup is shown in Figure 6-9.

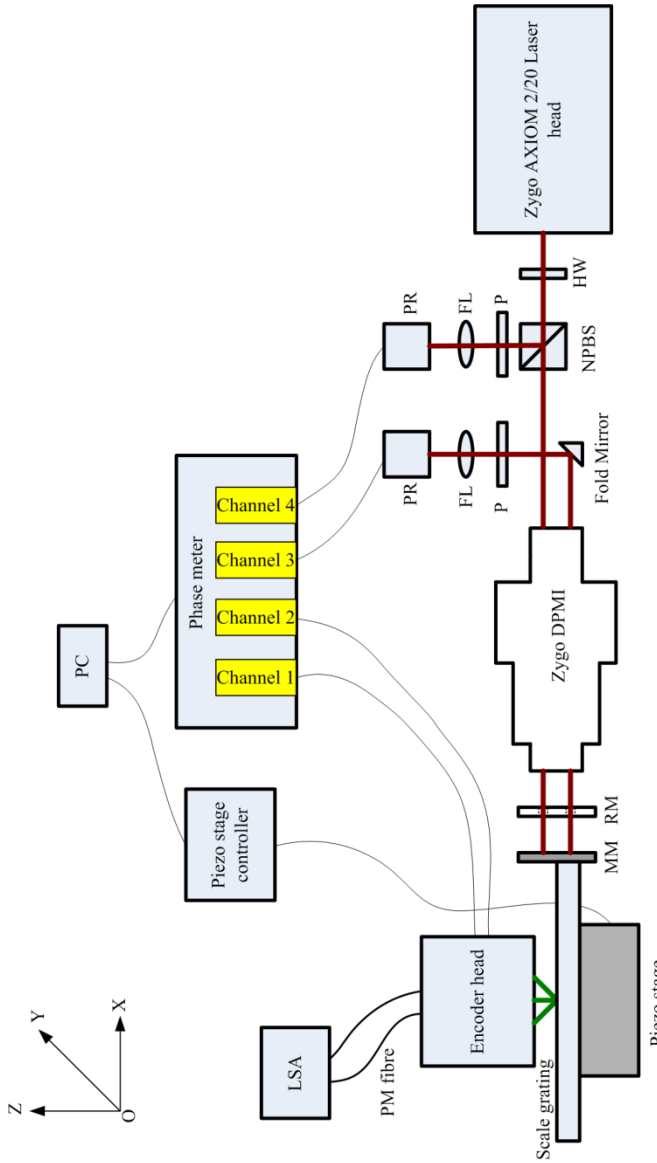

Figure 6-8. Schematic of the setup of comparison measurement between the DIHEI encoder and an interferometer; HW is half wave plate, NPBS is

non-polarization beam splitter, P is polarizer, FL is focusing lens, PR is photoreceiver, Zygo DPMI is the Differential Plane Mirror Interferometer module 7105 produced by the company Zygo, RM is the Zygo Reference Mirror Displacement-Model 7017, MM is the measurement mirror of the interferometer.

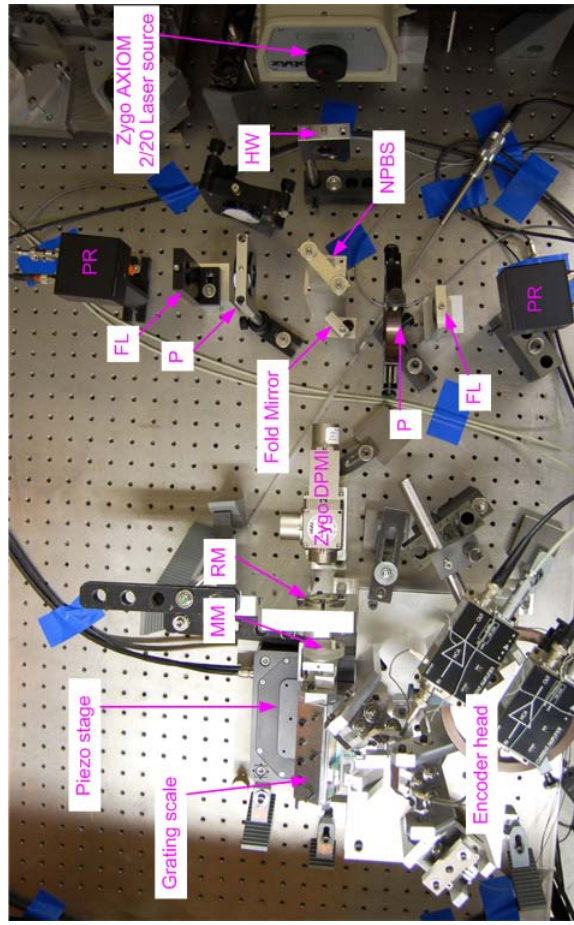

Figure 6-9. The photography of the opto-Mechanical parts of the comparison setup; HW is half wave plate, NPBS is non-polarization beam splitter, P is polarizer, FL is focusing lens, PR is photoreceiver, Zygo DPMI is the

Differential Plane Mirror Interferometer module 7105, RM is the Zygo Reference Mirror Displacement-Model 7017, MM is the measurement mirror of the interferometer.

During the comparison measurement, the sampling rate of the phase meter was 100 MHz and the averaging window length was 1800 for both DIHEI encoder and the interferometer, which resulted in a data acquisition rate of 55.556 kHz for both systems. The piezo stage moved repeatedly back and forth in X-direction with amplitude of 25 μm and repetition frequency of 0.1 Hz, which means that the piezo stage moved in a speed of 10 μm/s; this movement was measured by the DIHEI encoder and the interferometer simultaneously, as shown in Figure 6-10.

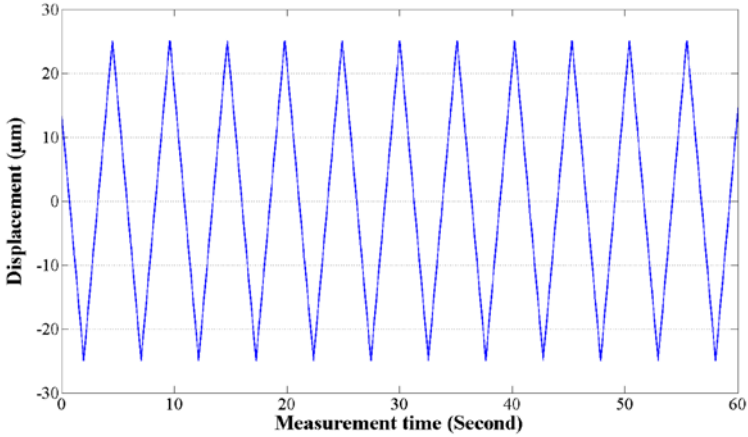

Figure 6-10. The piezo stage movement (in X-direction) measured by the DIHEI encoder and the interferometer simultaneously.

Due to the unrecoverable dislocation of a capacitance sensor inside the piezo stage, during movement the stage showed up to 400 μradian of pitch deviation, up to 20 μradian of yaw and roll deviations

as well as more than ±10 nm of repeatability, according to the reading of the PI NanoCapture (application software of the piezo stage). The DIHEI encoder and the interferometer had different sensitivities to the angular deviations of the piezo stage movement. To reduce the influence introduced by the angular deviations and repeatability of the piezo stage, only the comparison measurement data, which was corresponding to the displacements from -15 μm to 15 μm of rising slopes in Figure 6-10, were used to determine the periodic nonlinearity of the DIHEI encoder. Since when the piezo stage moved close to the turning points and at the falling slopes, it showed stronger angular deviations and larger fluctuation of moving speed. Even in those selected displacement ranges at the rising slopes, there are still obvious influences of the stage angular deviations, an example is shown in Figure 6-11. Figure 6-11 shows the measurement difference between the DIHEI encoder and the interferometer when the piezo stage moved from -15 μm to 15 μm at a rising slope; the stronger fluctuation of the measurement difference during the stage moved from -11 to -3 μm was resulted from the bigger angular deviations of the piezo stage at that displacement range, which was indicated by the reading of the aforementioned PI NanoCapture. The cosine error between the two systems was already removed, since the cosine error and other linear errors would not affect the determination of the encoder periodic nonlinearities.

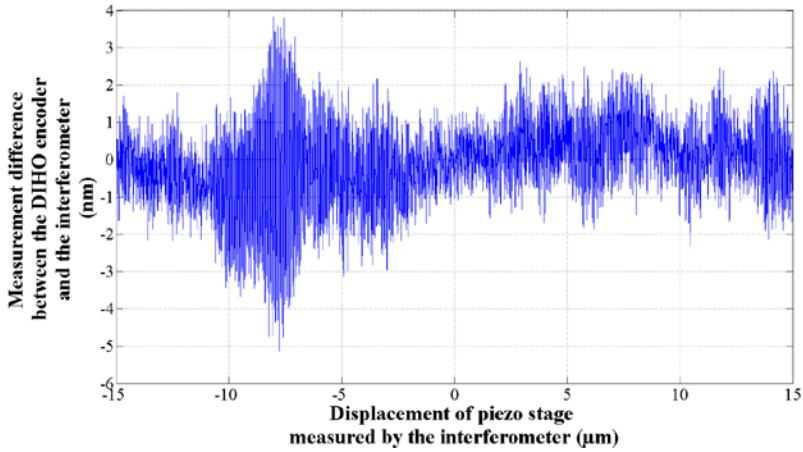

Figure 6-11. An example of the measurement difference between the DIHEI encoder and the interferometer during the piezo stage moved from -15 μm to 15 μm at a rising slope.

To identify the periodic nonlinearity of the DIHEI encoder, a fast Fourier transform of the measurement differences, which correspond to all the displacements from -15 μm to 15 μm of all the rising slopes, was performed, as shown in Figure 6-12. The nominal signal period of the DIHEI encoder is 416.667 nm and that of the interferometer is 158.248 nm. According to the nominal-constant moving speed of the piezo stage and the signal periods of the DIHEI encoder and the interferometer, the first and the second order of the nominal DIHEI-encoder-periodic-nonlinearity frequencies are 24 Hz and 48 Hz respectively, the corresponding signal periods are 416.667 nm and 208.333 nm respectively; the first and the second order nominal frequencies of the interferometer periodic nonlinearity are 63.19 Hz and 126.4 Hz respectively, and the corresponding signal periods are 158.248nm and 79.124nm respectively. As shown in Figure 6-12, the

first and second order periodic nonlinearities of the interferometer are ±0.236 nm and ±0.309 nm respectively. The first order periodic nonlinearity of the DIHEI encoder is 21 pm. And around 48 Hz / 208.333 nm which correspond to the second order periodic nonlinearity of the DIHEI encoder signal, there is no obvious peak. There are two peaks at 37.7Hz and 45.14Hz; for the peak at 37.7Hz, it had a amplitude of 27 pm and kept unchanged when the moving speed of the piezo stage was changed; and for the peak at 45.14Hz, it just showed up in some measurement results, which meant that it didn't correspond to a systematic error; the concrete reasons for those phenomena need to be further identified, although we currently suspect that the piezo stage be responsible for them. In Figure 6-12 (b), there are also some peaks which have signal periods less than 70 nm (the strongest peak has a length period of 57.83nm). Those peaks don't have integer relation with the period of the DIHEI encoder and the interferometer; therefore they are not the periodic nonlinearities of the DIHEI encoder and the interferometer. Under current investigation, those peaks are still caused by the piezo stage, the reason is following: when each of the amplitude spectra based on one of the rising slopes shown in Figure 6-10, is examined one by one, the peaks which correspond to the periodic nonlinearities of the DIHO encoder and the interferometer are quite stable from amplitude spectrum to amplitude spectrum. But the peaks, which have periods less than 70 nm, fluctuate strongly from amplitude spectrum to amplitude spectrum, as shown in Figure 6-13.

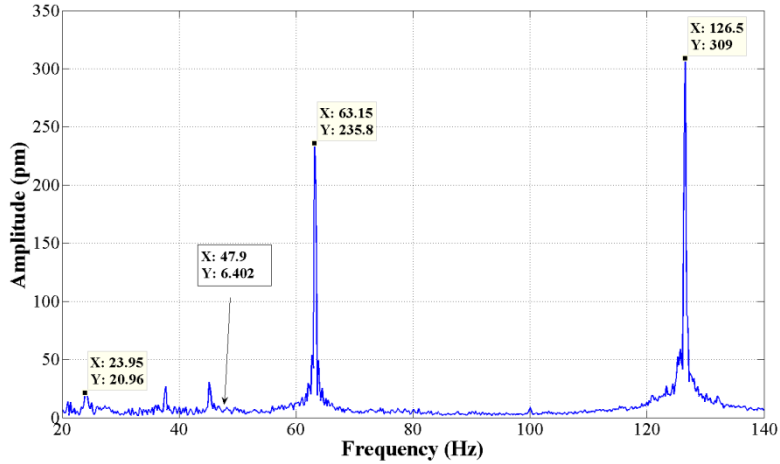

(a)

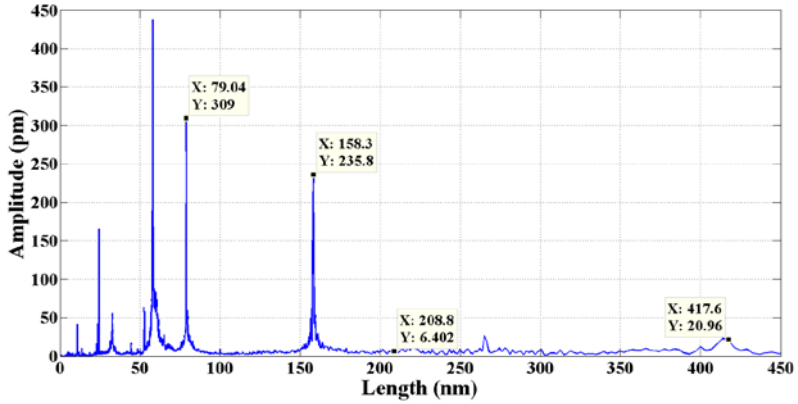

(b)

Figure 6-12. (a) Amplitude spectrum (from 20 Hz to 140 Hz) of the measurement differences corresponding to all the displacements from -15 μm to 15 μm of all the rising slopes, (b) The horizontal axis of the amplitude spectrum in (a) is converted into length(nm); X: horizontal axis, Y: vertical axis.

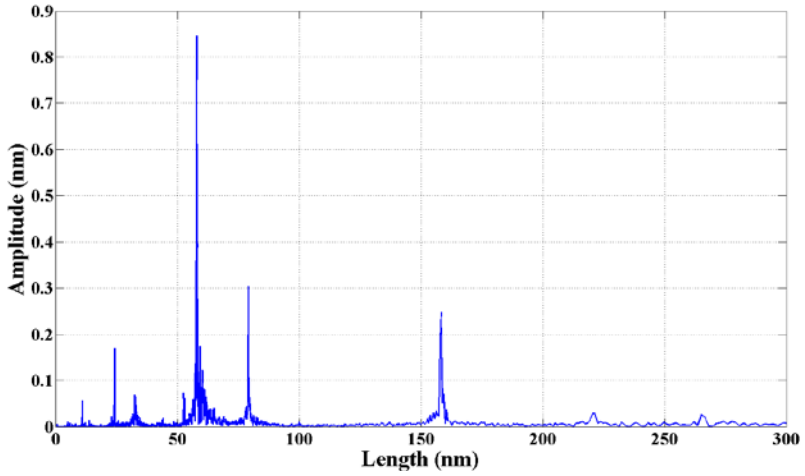

(a)

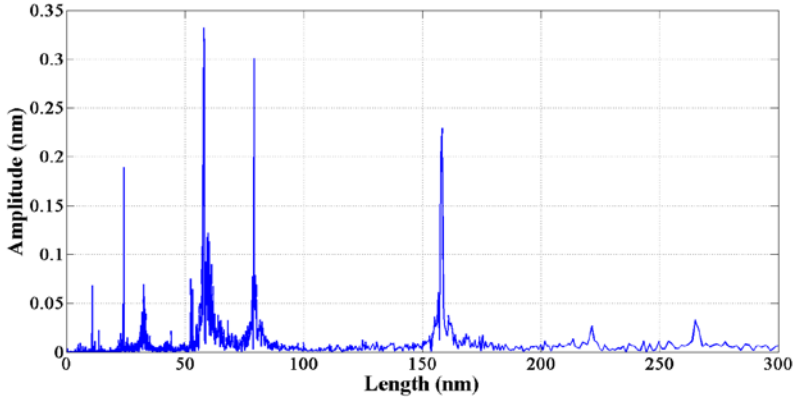

(b)

Figure 6-13. Amplitude spectra based on a single rising slope shown in Figure 6-10: (a) based on the fourth rising slope, (b) based on the fifth rising slope.

Under current situation, it is reasonable to draw a conclusion that the periodic nonlinearity of the DIHEI encoder is less than ±30 pm. But in

the future, to more accurately determine the periodic nonlinearity of the DIHEI encoder, a better linear stage and a much more accurate linear displacement measurement system than the current interferometer are required.

6.4. Measurement uncertainties analysis

The measurement uncertainties of a heterodyne encoder can be classified into two groups: position-independent uncertainties and position-dependent uncertainties, as listed in Table 6-1. Here the term ‘position dependency’ is used to indicate whether the resulting measurement uncertainties relate to the relative position between encoder head and grating scale in the measurement direction or not. The position-independent uncertainties of the DIHEI encoder, except those introduced by the deviations of other axes, can be represented by its system stability.

The position-dependent uncertainties can be further divided into two categories: periodic nonlinearities and the rest. Optics errors will result in periodic nonlinearities whose periods have integer-time relations with that of the encoder signal. The imperfections of the grating scale can cause both periodic nonlinearities and the rest. But the period of the periodic nonlinearities, which result from the imperfections of the grating scale, don’t necessarily have integer-time relations with that of the encoder signal. For the DIHEI encoder, the position-dependent uncertainty introduced by the optics errors had been determined to be less than ±30 pm; however the position-dependent uncertainty introduced by the imperfections of the grating scale was not measured in this work. There are two following

reasons for that: firstly, the grating scale, which was used in this experiment, is not specially manufactured for the optical encoder; secondly, the imperfection of the grating scale is as-built one which is stable enough if the suitable substrate material is chosen. And for the application in the wafer stages of lithography machine tools, the measurement uncertainty introduced by the as-built imperfection of grating scale can be calibrated. For the cosine error, it is a linear error and can be compensated.

The position-independent uncertainties of the DIHEI encoder can be further reduced, when the mechanical parts are optimized and the encoder head is miniaturized. Therefore, it is believed that the design of the DIHEI encoder has the potential to meet the requirements of those wafer stage metrology systems which require the overall measurement uncertainty and repeatability of several nanometers even sub-nanometer, no matter those wafer stages work in aerial or vacuum environment.

Table 6-1. Contributors to the measurement uncertainties of a heterodyne encoder.

Contributor	**Position dependency**
Electronics noises	Position-independent
Quantization error	
Laser source fluctuation	
Ambient environment fluctuation [a]	
Deviations of other axes (e.g. Abbe error)	
Optics errors [b]	Position-dependent
Imperfection and contaminations of grating scale	

Cosine error	
[a] Like vibrations, temperature and pressure fluctuations.	
[b] The imperfections of the optical elements, multi-reflections in the encoder head and so on.	

6.5. Conclusion

An interferometric heterodyne encoder was demonstrated with periodic nonlinearity of less than ±30 pm (without any correction) and system stability of 38 pm (standard deviation) and 100 pm (standard deviation) over 30 seconds and one hour respectively. Based on the measurement uncertainties analysis, it is believed that the design of the DIHEI encoder has the potential to meet the requirements of those wafer stage metrology systems which require the overall measurement uncertainty and repeatability of several nanometers even sub-nanometer, no matter those wafer stages work in aerial or vacuum environment.

References

[6.1.] P Köchert, J Flügge, Ch Weichert, R Köning and E Manske. Phase measurement of various commercial heterodyne He-Ne-laser interferometers with stability in the picometer regime. Measurement Science and Technology. 2012; 23: 074005

[6.2.] C Weichert, P Köchert, R Köning, J Flügge, B Andreas, U Kuetgens and A Yacoot. A heterodyne interferometer with

periodic nonlinearities smaller than ±10pm. Measurement Science and Technology. 2012, 23: 094005

[6.3.] Zygo corporation 1988 AXIOM 2/20 LASER MEASUREMENT SYSTEM Operation and Reference Manual OMP-0220

7. Conclusion and outlook

7.1. Conclusion

A TCHOI encoder was devised and built up. If a home built phase meter based on fast ADCs together with off-line Heydemann correction were employed, its channel1 exhibited a periodic nonlinearity of less than ± 10 pm; in the case a HEIDENHAIN EIB741 was used as its DPEAS, a synthetic periodic nonlinearity of ± 50 pm in its channel1, a synthetic periodic nonlinearity of ± 150 pm in its channel2 and a synthetic periodic nonlinearity of ± 70 pm in its channel3 were observed. The poorer performance of its channel2 and channel3 were due to their lower signal contrast which can be improved optically or electronically in the future. This TCHOI encoder also can provide an opportunity to investigate the suspected different measurement uncertainties of the three channels, which result from the corresponding correlations between ICGS and the different diffraction orders.

A novel two-dimensional interferometric homodyne encoder was put forward. Its scale grating was a one-dimensional grating. Along X-axis, its measurement standard was the period of the grating scale; along Z-axis, the measurement standard was the synthesis of the period of the grating scale and the wavelength of the laser. Its principle was proven by the proof-of-principle experiment.

A DIHEI encoder was designed and developed. It was demonstrated with periodic nonlinearity of less than ±30 pm (without any correction) and system stability of 38 pm (standard deviation) and 100 pm (standard deviation) over 30 seconds and one hour respectively. Based on the measurement uncertainties analysis, it is believed that the design of the DIHEI encoder has the potential to meet the requirements of those wafer stage metrology systems which require the overall measurement uncertainty and repeatability of several nanometers even sub-nanometer, no matter those wafer stages work in aerial or vacuum environment.

In comparison with all the found reported encoders which are briefly described in section 3.6, the TCHOI encoder and the DIHEI encoder are demonstrated with better performance, especially with respect to the periodic nonlinearity and system stability. For the two-dimensional (one is in-plane X-axis another one is out-of-plane Z-axis) interferometric homodyne encoder, it employs one-dimensional grating as grating scale; and its Z-axis measurement standard is the synthesis of period of grating scale and the wavelength of laser. In principle this two-dimensional interferometric encoder has the potential to achieve better measurement uncertainties along both axes, compared to those two-dimensional encoders which

theoretically are combinations of one-dimensional encoders and displacement interferometers.

7.2. Outlook

ICGS: The measurement standard of encoder is the period of the grating scale. When encoder is required to have sub-nanometer measurement uncertainty, the influence of ICGS will become non-negligible. To reduce the influence of the ICGS, one possible solution lies in the selection of different diffraction orders as described in chapter 4. To further investigate in this direction, following prerequisite works need to be done:

- Define the general forms and dimensions of the ICGS, with respect to the nominal parameters of the grating scale and the wavelength of the working light;
- Perform the strict photonic simulation about the possible different sensitivities of the different diffraction orders to the ICGS;
- Optimize the TCHOI encoder toward the equal performances among its three channels.

Six degree-of-freedom encoder systems: For the applications in nanometer-and-below precision engineering, six degree-of-freedom (DOF) measurements are necessary not only for six DOF position controlling but also for position error compensation along a certain axis. Decoupling a DOF measurement from the rest five DOF measurements is not an easy task but should be accomplished in the near future.

Better position correction algorithm: Heydemann correction only corrects the first and second order periodic nonlinearities. But to further reduce the periodic nonlinearities, a better correction method needs to be developed.

Abbe-error-free line design: Compared with the displacement interferometer, it is not easy to align an encoder according to Abbe principle. To overcome this disadvantage of the encoder, one ideal situation is that the encoder's Abbe-error-free line is designable. To achieve this, following two challenges need to be conquered first:

- How to design the encoder Abbe-error-free line?
- Is there at least an encoder solution which can meet all the requirements including the requirement on its Abbe-error-free line?

Using ray tracing to identify the Abbe-error-free line is shown in Appendix B. But to answer these two questions, a possible direction is to develop an encoder design program which is based on ray tracing and optimization, similar to the traditional optical design software like ZEMAX and Code V. One of the main features of the prospective encoder design software is its Abbe-error-free line design function which the traditional optical design softwares don't have.

8. Acknowledgment

This thesis work would not have been possible without the support of many people. First I would like to extend my sincere thank to my supervisors Dir. U. Prof. Dr. Harald Bosse, Prof. Dr.-Ing. Rainer Tutsch and Dr. Jens Flügge for providing me an opportunity to do my PhD thesis work at Physikalisch Technische Bundesanstalt (PTB). Deep gratitude is due to Dr. Jens Flügge for his care, guidance, advice and the inspiring discussions during my more than three years working at PTB.

As a student member of Braunschweig International Graduate School of Metrology (IGSM) Technische Universität Braunschweig, I benefit not only from its financial support, but also from its world top class of education in the metrology field. Frontier researches reported by the renowned scientists in summer schools, lectures about basic knowledge and skills provided by experts and professors, field trips to companies and so on all these enrich my experience of PhD study.

There are two guys without whose helps I still can carry out my thesis work but with more difficulties and longer time. They are my colleagues Christoph Weichert and Paul Köchert; thank you guys for always-ready help not only in my work but also in my private life, which is important for the person like me who rushed into Germany even without basic knowledge of German letters. Many thanks to Dr. Li, the course director of IGSM, Thank you for your always warm-hearted help in my work and my private life! During my work, Dr. Rainer Köning gave me quite lot of help, thanks! I also want to thank my colleagues Mr. Manfred Dähn, Mr. Karsten Fromm, Mr. Eugen Schötka, Mr. Michael Voigt, Ms. Christina Müller and Ms. Gerhild Borek for the support and help in my work.

In Chinese traditional culture, it is not a common practice for the children to say ‘thanks’ to their parents directly. But here I want to exclaim my thanks to my parents, thanks for your immense love and care. My wife sacrificed her own career to support me to do my PhD in Germany; she also tries to take care of my son by herself to let me to concentrate on my PhD work, thanks darling!

Finally, I dedicate this dissertation to my grandmother.

9. Appendix A

Jones matrices for relevant optical elements:

Octadic-wave plate (45°): $\frac{1}{2}\begin{bmatrix} 1+e^{i\frac{\pi}{4}} & 1-e^{i\frac{\pi}{4}} \\ 1-e^{i\frac{\pi}{4}} & 1+e^{i\frac{\pi}{4}} \end{bmatrix}$;

Quarter-wave plate (45°): $\frac{\sqrt{2}}{2}\begin{bmatrix} 1 & -i \\ -i & 1 \end{bmatrix}$;

Half-wave plate (22.5°): $-\frac{\sqrt{2}i}{2}\begin{bmatrix} 1 & 1 \\ 1 & -1 \end{bmatrix}$;

Polarizer (0°): $\begin{bmatrix} 1 & 0 \\ 0 & 0 \end{bmatrix}$;

Polarizer (180°): $\begin{bmatrix} 0 & 0 \\ 0 & 1 \end{bmatrix}$;

Polarizer (45°): $\frac{1}{2}\begin{bmatrix} 1 & 1 \\ 1 & 1 \end{bmatrix}$;

Polarizer (135°): $\frac{1}{2}\begin{bmatrix} 1 & -1 \\ -1 & 1 \end{bmatrix}$.

Jones vector of linear-polarization incidence beam: $\begin{bmatrix} 1 \\ 0 \end{bmatrix}$.

Channel1:

Electromagnetic field of beam (1, 1_L, -1):

$$E1_1 = \frac{1}{4}\begin{bmatrix} 1+e^{i\frac{\pi}{4}} & 1-e^{i\frac{\pi}{4}} \\ 1-e^{i\frac{\pi}{4}} & 1+e^{i\frac{\pi}{4}} \end{bmatrix}\begin{bmatrix} 1+e^{i\frac{\pi}{4}} & 1-e^{i\frac{\pi}{4}} \\ 1-e^{i\frac{\pi}{4}} & 1+e^{i\frac{\pi}{4}} \end{bmatrix}\begin{bmatrix} e^{i2\phi} \\ 0 \end{bmatrix} = \frac{e^{i2\phi}}{2}\begin{bmatrix} 1+i \\ 1-i \end{bmatrix}$$

Where Φ is the phase introduced by the relative movement between grating scale and the encoder head.

Electromagnetic field of beam (-1, -1_R, 1):

$$E1_{-1} = \frac{1}{2}\begin{bmatrix} 1 & -i \\ -i & 1 \end{bmatrix}\begin{bmatrix} 1 & -i \\ -i & 1 \end{bmatrix}\begin{bmatrix} e^{-i2\phi} \\ 0 \end{bmatrix} = e^{-i2\phi}\begin{bmatrix} 0 \\ -i \end{bmatrix}.$$

After beam (1, 1_L, -1) and beam (-1, -1_R, 1) superimposing and transmitting through a 45° oriented polarizer:

$$E1_{90^\circ} = \frac{1}{4}\left(e^{i2\phi} - ie^{-i2\phi}\right).$$

Therefore the detected signal detected by detector 1 (90°) is:

$$I1_{90^\circ} = \frac{1}{8} - \frac{1}{8}\sin(4\phi).$$

After beam (1, 1_L, -1) and beam (-1, -1_R, 1) superimposing and being reflected by a 45° oriented polarizer:

$$E1_{0^\circ} = \frac{1}{4}\left(ie^{i2\phi} + ie^{-i2\phi}\right).$$

Therefore the detected signal detected by detector 1 (0°) is:

$$I1_{0^\circ} = \frac{1}{8} + \frac{1}{8}\cos(4\phi).$$

Channel2:

Electromagnetic field of beam (1, 1_L, 0):

$$E2_1 = \frac{\sqrt{2}}{8}\begin{bmatrix} 1 & -i \\ -i & 1 \end{bmatrix}\begin{bmatrix} 1+e^{i\frac{\pi}{4}} & 1-e^{i\frac{\pi}{4}} \\ 1-e^{i\frac{\pi}{4}} & 1+e^{i\frac{\pi}{4}} \end{bmatrix}\begin{bmatrix} 1+e^{i\frac{\pi}{4}} & 1-e^{i\frac{\pi}{4}} \\ 1-e^{i\frac{\pi}{4}} & 1+e^{i\frac{\pi}{4}} \end{bmatrix}\begin{bmatrix} e^{i\phi} \\ 0 \end{bmatrix} = \frac{\sqrt{2}}{8}\begin{bmatrix} 0 \\ e^{i\phi} \end{bmatrix}.$$

Electromagnetic field of beam (-1, -1_R, -2):

$$E2_{-1} = \frac{1}{8}\begin{bmatrix} 1 & -i \\ -i & 1 \end{bmatrix}\begin{bmatrix} 1 & -i \\ -i & 1 \end{bmatrix}\begin{bmatrix} 1 & -i \\ -i & 1 \end{bmatrix}\begin{bmatrix} e^{-i3\phi} \\ 0 \end{bmatrix} = \frac{1}{8}\begin{bmatrix} -ie^{-i3\phi} \\ e^{-i3\phi} \end{bmatrix}.$$

After beam (1, 1_L, 0) and beam (-1, -1_R, -2) superimposing and transmitting through a 45° oriented polarizer:

$$E2_{90^\circ} = \frac{1}{8}\left[\sqrt{2}e^{i\phi} + (1-i)e^{-i3\phi}\right].$$

Therefore the detected signal detected by detector 2 (90°) is:

$$I2_{90^\circ} = \frac{1}{16} + \frac{1}{16}\cos\left(4\phi + \frac{\pi}{4}\right).$$

After beam (1, 1_L, 0) and beam (-1, -1_R, -2) superimposing and being reflected by a 45° oriented polarizer:

$$E2_{0^\circ} = -\frac{1}{8}\left[\sqrt{2}e^{i\phi} + (1+i)e^{-i3\phi}\right].$$

Therefore the detected signal detected by detector 2 (0°) is:

$$I2_{0^\circ} = \frac{1}{16} + \frac{1}{16}\sin\left(4\phi + \frac{\pi}{4}\right).$$

Channel3:

Electromagnetic field of beam (1, 1_L, 2):

$$E3_1 = \frac{1}{8}\begin{bmatrix} 1+e^{i\frac{\pi}{4}} & 1-e^{i\frac{\pi}{4}} \\ 1-e^{i\frac{\pi}{4}} & 1+e^{i\frac{\pi}{4}} \end{bmatrix}\begin{bmatrix} 1+e^{i\frac{\pi}{4}} & 1-e^{i\frac{\pi}{4}} \\ 1-e^{i\frac{\pi}{4}} & 1+e^{i\frac{\pi}{4}} \end{bmatrix}\begin{bmatrix} 1+e^{i\frac{\pi}{4}} & 1-e^{i\frac{\pi}{4}} \\ 1-e^{i\frac{\pi}{4}} & 1+e^{i\frac{\pi}{4}} \end{bmatrix}\begin{bmatrix} e^{i3\phi} \\ 0 \end{bmatrix} =$$

$$\frac{\sqrt{2}}{4}e^{i3\phi}\begin{bmatrix} 1-i+(1+i)e^{i\frac{\pi}{4}} \\ 1-i-(1+i)e^{i\frac{\pi}{4}} \end{bmatrix}.$$

Electromagnetic field of beam (-1, -1_R, 0):

$$E3_{-1} = \frac{1}{2}\begin{bmatrix} 1+e^{i\frac{\pi}{4}} & 1-e^{i\frac{\pi}{4}} \\ 1-e^{i\frac{\pi}{4}} & 1+e^{i\frac{\pi}{4}} \end{bmatrix}\begin{bmatrix} 0 \\ e^{-i\phi} \end{bmatrix} = \frac{e^{-i\phi}}{2}\begin{bmatrix} 1-e^{i\frac{\pi}{4}} \\ 1+e^{i\frac{\pi}{4}} \end{bmatrix}.$$

After beam (1, 1_L, 2) and beam (-1, -1_R, 0) superimposing, passing through a 45° oriented half-wave plate and transmitting through a 0° oriented polarizer:

$$E3_{90^\circ} = \frac{1}{2}\left[\sqrt{2}e^{i3\phi}(1-i) + 2e^{-i\phi}\right].$$

Therefore the detected signal detected by detector 3 (90°) is:

$$I3_{90^\circ} = 2 + 2\sin\left(4\phi + \frac{\pi}{4}\right).$$

After beam (1, 1_L, 2) and beam (-1, -1_R, 0) superimposing, passing through a 45° oriented half-wave plate and transmitting through a 90° oriented polarizer:

$$E3_{0^\circ} = \frac{1}{2}\left[\sqrt{2}e^{i3\phi}(1+i)e^{i\frac{\pi}{4}} - 2e^{i\frac{\pi}{4}}e^{-i\phi}\right].$$

Therefore the detected signal detected by detector 3 (0°) is:

$$I3_{0^\circ} = 2 + 2\cos\left(4\phi + \frac{\pi}{4}\right).$$

For each channel, there are only 0° and 90° optical quadrature signals; to adapt to the already available transimpedance amplifier which requires four quadrature signals, the 180° and 270° quadrature signals are attained through 180°- phase inversion of the relevant 0° and 90° optical quadrature signals.

10. Appendix B

In this thesis, the Abbe-error-free line is defined to have following two intrinsic characters:

1. When the measurement axes of interest are co-linear with the Abbe-error-free lines, there will be no Abbe errors any more. That is to say, on the Abbe-error-free lines, the Abbe errors are automatically compensated by the encoders themselves;
2. The Abbe-error-free axis is parallel to the scale axis, as shown in Figure B-1.

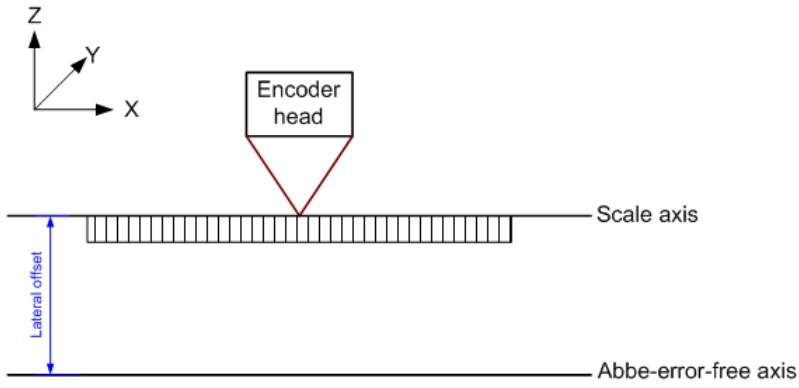

Figure B-1 Schematic of the Abbe-error-free axis of an encoder.

To determine the Abbe-error-free line of this TCHOI encoder, first a strict manual ray tracing must be carried out; this manual ray tracing will result in a big number of analytical relations. Therefore a numerical simulation needs to be performed to determine its Abbe-error-free line. In the following, channel1 of this TCHOI encoder is taken as an example to show this process.

As shown in Figure B-2, it is the manual ray tracing of the channel1 of this TCHOI encoder. The rotation of the grating scale around a random point can be converted into the linear combination of a rotation around another point and a lateral displacement which is orthogonal to its scale axis. And the TCHOI encoder is theoretically insensitive to the lateral displacement due to its symmetrical configuration. Therefore, in Figure B-2, the grating scale rotation point O is set on the extension line of the interfering beam (1, 1_L, -1) and beam (-1, -1_R, 1), when the grating scale is on its nominal orientation. The related constants and variables are listed in Table B-1

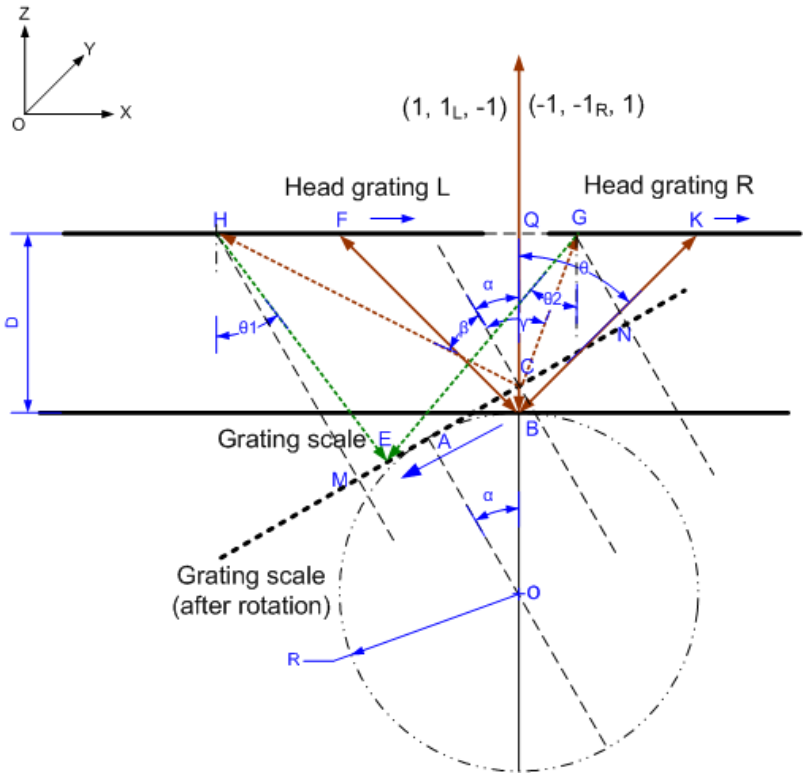

Figure B-2. Manual ray tracing of the channel1 of the TCHOI encoder.

Table B-1. Constants and variables.

Period of grating scale (ps)	833.33nm
Period of head grating (ph)	416.667nm
Lateral offset (R)	variable
Rotation angle (α)	[-1°, -1°] (supposed)
Wavelength (lamda)	532nm
Gap between Grating Scale and Head Grating (D)	70mm
β: +1 order diffraction angle (after rotation)	
γ: -1 order diffraction angle (after rotation)	

θ: ±1 diffraction angle (before rotation, normal position)	
θ1: diffraction angle @ HG of L;	
θ2: diffraction angle @ HG of R;	

Analytical relations:

- **Grating equations:**

  - **Grating Scale**

Sin (β) =lamda/ps+sin(α)

Sin (γ) = lamda/ps-sin (α)

Sin (θ) = lamda/ps

  - **Head Grating**

ph*(sin(α+ β)+sin(θ1)) = lamda

ph*(sin(γ- α)+sin(θ2)) = lamda

- **Geometry:**

  - **Grating Scale**

AC=R*tan(α); AC is the grating scale translation resulting from the rotation

α, which detected by the encoder..

BC= R/cos(α)-R;

(Relation from left head grating)

CH = (D-BC)/cos(α+ β)

CM = CH*sin (β)

HM = CH*cos(β)

EH = HM/cos(θ1- α)

EM = HM*tan (θ1- α)

EC1 = CM-EM (EC from left)

(Relation from right head grating)

CG = (D-BC)/cos(γ- α)

CN = CG*sin (γ)

GN = CG*cos(γ)

EG = GN/cos(θ2+ α)

EN = GN*tan (θ2+ α)

EC2 = EN-CN (EC from right)

EC1-EC2 (overlapping degree @SG ---two interfering beams)

- **Head Grating**

FQ = D*tan (θ)

HQ = (D-BC)*tan (α+ β)

HF = HQ-FQ

KQ = FQ = D*tan (θ)

GQ = (D-BC)*tan (γ- α)

KG = KQ - GQ

When grating scale is rotated by α around point o, two parts of phase change will be brought about accordingly, one part is due to the translation (AC) of grating scale (**Phase1**), another part is the OPL(optical path length) change with respect to the normal position (**Phase2**), as listed in Table B-2.

Table B-2. Resulting phase change.

	Phase1 Phase change due to the translation (AC)		**Phase2** Phase change due to OPL change
+1 Diffraction order (L)	@SG	-AC/ps*2π- (AC-EC1)/ps*2π	[CH+EH-2*D/cos(θ)]/lamda*2π
	@HG	-HF/ph*2 π	
-1 Diffraction order (R)	@SG	AC/ps*2π+ (AC-EC2)/ps*2π	[CG+EG-2*D/cos(θ)]/lamda*2π
	@HG	KG/ph*2 π	
Encoder		-2*AC/ps*2π-(2*AC-EC1- EC2)/ps*2π-(HF+KG)/ph*2 π	(CH+EH-CG-EG) /lamda*2π

When the overall phase (Phase1 + Phase2) is insensitive to the rotation α, the corresponding lateral offset R defines the location of

the Abbe-error-free line. According to the numerical simulation, the Abbe-error-free line of the channel1 is its scale axis.

11. List of acronyms, abbreviations and symbols

2DH	zweidimensionaler homodyner
2DHI	two-dimensional homodyne interferometric
3KH	dreikanaliger homodyner
AC	Alternating current
ADC	Analog-to-digital converter
AOM	acousto-optic modulator
BC	beam combiner

CD	Critical Dimension
CO2	Carbon dioxide
CPU	Central Processing Unit
D	Detector
DC	Direct current
DH	differentieller heterodyner
DIHEI	differential heterodyne interferometric
DOF	Degree-of-freedom
DPEAS	data processing electronics and application software
DSP	Digital Signal Processor
FFT	fast Fourier transform
FL	focusing lens
FPGA	Field-Programmable Gate Array
FS	Full Scale

HeNe	helium-neon
HW(λ/2)	half wave plate
IC	integrated circuit
ICGS	Imperfections and Contaminations of the Grating Scale
JCGM	Joint Committee for Guides in Metrology
LED	Light-emitting diode
LS	light source
LSA	light source assembly
LVDT	Linear Variable Differential Transformer
MM	measurement mirror
Nd:YAG	Neodymum-doped yttrium aluminum garnet
NPBS	non-polarization beam splitter
P	polarizer
PBS	polarization beam splitter

PLL	phase-locked loop
PM	polarization-maintaining
PN	periodische Nichtlinearität
PR	photoreceiver
RM	reference mirror
TCHOI	three-channel homodyne interferometric
Tran-Amp	transimpedance amplifier
WP	Wave plate
λ	wavelength
λ/4	Quarter-wave plate
λ/8	Octadic-wave plate
σ	Standard deviation